
Learning Where to Learn: Training Distribution Selection for Provable OOD Performance

Nicolas Guerra*
Cornell University
nmg64@cornell.edu

Nicholas H. Nelsen†
Massachusetts Institute of Technology
nnelsen@mit.edu

Yunan Yang‡
Cornell University
yunan.yang@cornell.edu

Abstract

Out-of-distribution (OOD) generalization remains a fundamental challenge in machine learning. Models trained on one data distribution often experience substantial performance degradation when evaluated on shifted or unseen domains. To address this challenge, the present paper studies the design of training data distributions that maximize average-case OOD performance. First, a theoretical analysis establishes a family of generalization bounds that quantify how the choice of training distribution influences OOD error across a predefined family of target distributions. These insights motivate the introduction of two complementary algorithmic strategies: (i) directly formulating OOD risk minimization as a bilevel optimization problem over the space of probability measures and (ii) minimizing a theoretical upper bound on OOD error. Last, the paper evaluates the two approaches across a range of function approximation and operator learning examples. The proposed methods significantly improve OOD accuracy over standard empirical risk minimization with a fixed distribution. These results highlight the potential of distribution-aware training as a principled and practical framework for robust OOD generalization.

1 Introduction

Out-of-distribution (OOD) generalization is a core obstacle for machine learning algorithms, particularly when the test-time data distribution differs significantly from that of training. Standard methods, such as empirical risk minimization (ERM) which focuses solely on minimizing the average loss over the training distribution, often overlook the complexities of distribution shift. This oversight can lead to substantial performance degradation when models are exposed to unseen or shifted domains. Such covariate shifts are common in scientific machine learning tasks such as solving infinite-dimensional inverse problems and operator learning for partial differential equations (PDEs).

This work proposes a framework for optimizing the training distribution to improve average-case OOD performance. Rather than accepting the limitations imposed by a fixed training distribution, the paper systematically investigates how the choice of training data influences generalization to target distributions. Guided by both theoretical insights and practical considerations, we develop a principled and computationally feasible strategy for *learning where to learn*: selecting the training data distribution that ensures robust performance across a specified family of test distributions.

Motivation. In nonlinear inverse problems like electrical impedance tomography (EIT), neural networks known as neural operators are used to learn maps between spaces of functions, e.g., from boundary voltage patterns to internal conductivity [19, 39, 42]. However, their success heavily depends on how the training data is chosen. In EIT, the input data comes from the so-called Dirichlet-to-Neumann (DtN) map Λ_a . It encodes how the voltage applied on the boundary of a domain leads

*Center for Applied Mathematics, Cornell University, Ithaca, NY 14853, USA.

†Department of Mathematics, Massachusetts Institute of Technology, Cambridge, MA 02139, USA.

‡Department of Mathematics, Cornell University, Ithaca, NY 14853, USA.

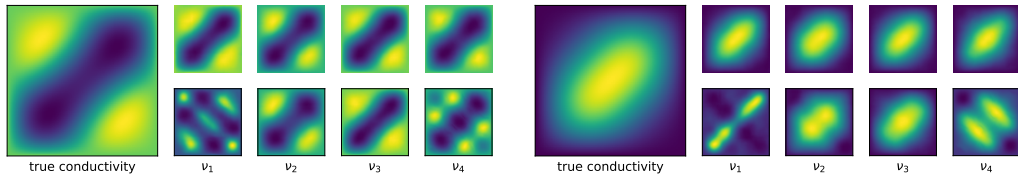


Figure 1: Two conductivity samples in EIT. The true conductivity is on the left of each panel, followed by predictions from models trained on four Dirichlet boundary condition distributions, ν_1 – ν_4 . Top row: in-distribution predictions; bottom row: OOD predictions. Refer to **SM D–E** for details.

to current flow and ultimately reveals information about the unknown conductivity a —the output data—inside the domain. We use input data pairs $\{(f_n, g_n)\}$ for training, where f_n is a voltage pattern applied at the boundary (a Dirichlet condition), and $g_n = \Lambda_a f_n$ is the resulting current response (a Neumann condition). These pairs are sampled from a probability distribution ν over the space of input voltages that we can choose freely. Crucially, this distribution ν has a significant impact on how well the model generalizes to new, unseen patterns. In Fig. 1, we explore this phenomenon using the Neural Inverse Operator (NIO) [39] and its variant; see **SM D–E** for details.

Contributions. The primary goal of this paper is to understand and optimize the role of training data distributions in improving OOD generalization for regression problems. Operator learning is a driving motivation, with a focus on challenging inverse problems such as EIT and parametrized PDE solution operators such as Darcy flow. Our main contributions are now listed.

- (C1) *Lipschitz-based OOD bounds.* We develop generalization bounds that connect OOD error to the Lipschitz continuity of the learned operator and quantitatively characterize how the Wasserstein mismatch between train and test distributions impact average-case performance.
- (C2) *Algorithmic strategies for training distribution optimization.* Motivated by the theory, we propose two label-dependent algorithms for actively optimizing the training distribution: bilevel optimization targeting average-case OOD risk and a computationally efficient alternative that minimizes an upper risk bound; both outperform nonadaptive ERM.
- (C3) *Empirical demonstration of distributional effects in operator learning.* Our numerical experiments demonstrate that the choice of training data distribution significantly influences generalization error in both forward and inverse operator learning tasks, consistent with the theoretical insights. Additionally, we showcase the effectiveness and efficiency of the two proposed algorithms in actively optimizing the training data distribution.

Related work. OOD generalization [37] connects to active learning, optimal experimental design (OED), and robust domain generalization. Active learning [16, 49, 55] improves model performance by selectively querying informative samples based on criteria like uncertainty or diversity. However, these methods operate reactively on unlabeled datasets during training, without addressing the proactive optimization of the initial training distribution. In contrast, our work emphasizes the systematic design of training distributions to improve robustness to distribution shifts, particularly in operator learning tasks like inverse problems and surrogate modeling. OED similarly focuses on distribution selection but within a statistical or Bayesian framework [6, 20, 21, 26]. Classical methods, such as A-optimality and D-optimality, aim to reduce estimation error, while Bayesian and sequential designs adaptively balance exploration and exploitation. Although these approaches focus on parameter inference or uncertainty reduction, our work departs by targeting training distribution optimization for minimizing OOD errors, which is not a commonly considered design principle in OED. Finally, our work aligns with robust domain generalization efforts, including distributionally robust optimization (DRO) [33, 45] and invariant risk minimization (IRM) [5, 28, 34, 56]. While DRO minimizes worst-case risk over predefined groups and IRM enforces invariance across domains, both approaches focus on robustness during training rather than optimizing the training data distribution itself. In contrast, we propose a novel framework that actively designs training distributions, guided by theoretical bounds and bilevel optimization, to address OOD challenges in regression problems.

Outline. This paper is organized as follows. Sec. 2 provides the necessary background. Sec. 3 establishes motivating theoretical results. Sec. 4 proposes two implementable data distribution

selection algorithms. Sec. 5 performs numerical studies and Sec. 6 gives concluding remarks. Details about derivations and numerical implementation are deferred to the supplementary material (SM).

2 Preliminaries

This section sets the notation, provides essential background on key mathematical concepts, and reviews the framework of operator learning. **SM A** contains additional reference material.

Notation. This paper works with an abstract input space $(\mathcal{U}, \langle \cdot, \cdot \rangle_{\mathcal{U}}, \|\cdot\|_{\mathcal{U}})$ and output space $(\mathcal{Y}, \langle \cdot, \cdot \rangle_{\mathcal{Y}}, \|\cdot\|_{\mathcal{Y}})$, both assumed to be real separable Hilbert spaces. We often drop the subscripts on norms and inner products when the meaning is clear from the context. Unless otherwise stated, \mathcal{U} or \mathcal{Y} could be infinite-dimensional. We denote the Lipschitz constant of a map $F: \mathcal{U} \rightarrow \mathcal{Y}$ by $\text{Lip}(F) := \sup_{u \neq u'} \|F(u) - F(u')\|_{\mathcal{Y}} / \|u - u'\|_{\mathcal{U}}$. For any element ζ of a metric space, the Dirac probability measure assigning unit mass to ζ is written as δ_{ζ} . For $p \in [1, \infty]$, (Bochner) $L^p_{\mu}(\mathcal{U}; \mathcal{Y})$ spaces are defined in the usual way. Let $m_p: \mathcal{P}(\mathcal{U}) \rightarrow \mathbb{R}_{\geq 0} \cup \{\infty\}$ denote the uncentered p -th moment defined by $\mu \mapsto m_p(\mu) := \mathbb{E}_{u \sim \mu} \|u\|_{\mathcal{U}}^p$. We say that a probability measure μ belongs to $\mathcal{P}_p(\mathcal{U})$ if $m_p(\mu) < \infty$. We often work with Gaussian measures $\mathcal{N}(m, \mathcal{C}) \in \mathcal{P}_2(\mathcal{U})$, where $m \in \mathcal{U}$ is the mean and $\mathcal{C}: \mathcal{U} \rightarrow \mathcal{U}$ is the symmetric trace-class positive semidefinite covariance operator; see [14, App. A.3] for details in the infinite-dimensional setting.

Background. We review several key concepts that frequently appear in this work.

The *pushforward operator* maps a measure from one measurable space to another via a measurable map. Specifically, given measure spaces (X, \mathcal{B}_X, μ) and (Y, \mathcal{B}_Y, ν) and a measurable map $T: X \rightarrow Y$, the pushforward operator $T_{\#}$ assigns to μ a measure $T_{\#}\mu$ on Y defined by $T_{\#}\mu(B) = \mu(T^{-1}(B))$ for all $B \in \mathcal{B}_Y$, where $T^{-1}(B) = \{x \in X \mid T(x) \in B\}$ is the pre-image of B . Intuitively, $T_{\#}$ redistributes the measure μ on X to a measure $T_{\#}\mu$ on Y following the structure of the map T .

Definition 2.1 (p -Wasserstein distance). Consider probability measures μ and ν on a metric space (X, d) with finite p -th moments, where $p \in [1, \infty)$. Define the set of all couplings $\Gamma(\mu, \nu) := \{\gamma \in \mathcal{P}(X \times X) \mid (\pi^1)_{\#}\gamma = \mu, (\pi^2)_{\#}\gamma = \nu\}$, where $\pi^1(x, y) = x$, $\pi^2(x, y) = y$, and $\mathcal{P}(X \times X)$ is the set of probability measures over $X \times X$. The p -Wasserstein distance between μ and ν is $W_p(\mu, \nu) := (\inf_{\gamma \in \Gamma(\mu, \nu)} \int_{X \times X} d(x, y)^p \gamma(dx, dy))^{1/p}$.

The cases of $p = 1$ and $p = 2$ are often considered, corresponding to the W_1 and W_2 metrics [54]. The case when μ and ν are both Gaussian and X is a Hilbert space is also used frequently.

We will use the notion of random measure [27] to quantify OOD generalization error in Secs. 3–4.

Definition 2.2 (random measure). Let $(\Omega, \mathcal{F}, \mathbb{P})$ be a probability space, and let (M, \mathcal{B}) be a measurable space. A *random measure* on M is a map $\Xi: \Omega \rightarrow \mathcal{P}(M)$, $\Xi(\omega) := \mu_{\omega}$, such that for every $A \in \mathcal{B}$, the function $\omega \mapsto \mu_{\omega}(A)$ is a random variable, i.e., measurable from (Ω, \mathcal{F}) to $(\mathbb{R}_{\geq 0}, \mathcal{B}(\mathbb{R}))$.

Operator learning. Operator learning provides a powerful framework for approximating mappings $\mathcal{G}^*: \mathcal{U} \rightarrow \mathcal{Y}$ between function spaces. It plays an increasingly pivotal role for accelerating forward and inverse problems in the computational sciences [9, 29, 30, 41]. As in traditional regression, the learned operator $\mathcal{G}_{\hat{\theta}}$ is parametrized over a set Θ and minimizes an *empirical risk*

$$\hat{\theta} \in \arg \min_{\theta \in \Theta} \frac{1}{N} \sum_{n=1}^N \|\mathcal{G}^*(u_n) - \mathcal{G}_{\theta}(u_n)\|_{\mathcal{Y}}^2. \quad (2.1)$$

The Hilbert norm in (2.1) and discretization-invariant architectures (e.g., DeepONet [36], Fourier Neural Operator (FNO) [32], NIO [39]) are points of departure from classical function approximation. In (2.1), $\{u_n\} \sim \nu^{\otimes N}$, where ν is the training distribution over input functions. The choice and properties of ν are crucial. An inadequately selected ν may result in $\mathcal{G}_{\hat{\theta}}(u)$ being a poor approximation to $\mathcal{G}^*(u)$ for $u \sim \nu'$, where $\nu' \neq \nu$ [1, 2, 10, 15, 31, 40, 43, 52]. The present work aims to improve such OOD generalization in both function approximation and operator learning settings.

3 Lipschitz theory for out-of-distribution generalization

This section studies how loss functions behave under distribution shifts and the implications of such shifts on average-case OOD accuracy. The assumed Lipschitz continuity of the target map and approximation class play a central role in the analysis.

Distribution shift inequalities. In the infinite data limit, the functional in (2.1) naturally converges to the so-called *expected risk*, which serves as a notion of model accuracy in this work. The following result forms the foundation for our forthcoming data selection algorithms in Sec. 4.

Proposition 3.1 (OOD generalization). *Let \mathcal{G}_1 and \mathcal{G}_2 both be Lipschitz continuous maps from Hilbert space \mathcal{U} to Hilbert space \mathcal{Y} . For any $\nu \in \mathcal{P}_1(\mathcal{U})$ and $\nu' \in \mathcal{P}_1(\mathcal{U})$, it holds that*

$$\mathbb{E}_{u' \sim \nu'} \|\mathcal{G}_1(u') - \mathcal{G}_2(u')\|_{\mathcal{Y}} \leq \mathbb{E}_{u \sim \nu} \|\mathcal{G}_1(u) - \mathcal{G}_2(u)\|_{\mathcal{Y}} + (\text{Lip}(\mathcal{G}_1) + \text{Lip}(\mathcal{G}_2))W_1(\nu, \nu'). \quad (3.1)$$

Moreover, for any $\mu \in \mathcal{P}_2(\mathcal{U})$ and $\mu' \in \mathcal{P}_2(\mathcal{U})$, it holds that

$$\mathbb{E}_{u' \sim \mu'} \|\mathcal{G}_1(u') - \mathcal{G}_2(u')\|_{\mathcal{Y}}^2 \leq \mathbb{E}_{u \sim \mu} \|\mathcal{G}_1(u) - \mathcal{G}_2(u)\|_{\mathcal{Y}}^2 + c(\mathcal{G}_1, \mathcal{G}_2, \mu, \mu')W_2(\mu, \mu'), \quad (3.2)$$

where $c(\mathcal{G}_1, \mathcal{G}_2, \mu, \mu')$ equals

$$(\text{Lip}(\mathcal{G}_1) + \text{Lip}(\mathcal{G}_2)) \sqrt{4(\text{Lip}(\mathcal{G}_1) + \text{Lip}(\mathcal{G}_2))^2 [\mathfrak{m}_2(\mu) + \mathfrak{m}_2(\mu')] + 16[\|\mathcal{G}_1(0)\|_{\mathcal{Y}}^2 + \|\mathcal{G}_2(0)\|_{\mathcal{Y}}^2]}.$$

See **SM B** for the proof. Provided that the maps \mathcal{G}_1 and \mathcal{G}_2 are Lipschitz, Prop. 3.1 shows that the functional $\mu \mapsto \mathbb{E}_{u \sim \mu} \|\mathcal{G}_1(u) - \mathcal{G}_2(u)\|_{\mathcal{Y}}$ is globally Lipschitz continuous in the W_1 metric. Similarly, the functional $\mu \mapsto \mathbb{E}_{u \sim \mu} \|\mathcal{G}_1(u) - \mathcal{G}_2(u)\|_{\mathcal{Y}}^2$ is *locally* Lipschitz continuous in the W_2 metric; in particular, it is Lipschitz on sets with uniformly bounded second moments. We remark that the Lipschitz map hypotheses in Prop. 3.1 are invoked for simplicity. Hölder continuity is also compatible with Wasserstein distances, and the preceding result can be adapted to hold under such regularity.

Average-case performance. OOD generalization performance may be quantified in several ways. This paper chooses *average-case accuracy* with respect to the law $\mathbb{Q} \in \mathcal{P}(\mathcal{P}(\mathcal{U}))$ of a random probability measure $\nu' \sim \mathbb{Q}$. For a ground truth map \mathcal{G}^* and any hypothesis \mathcal{G} , we strive for

$$\mathcal{E}_{\mathbb{Q}}(\mathcal{G}) := \mathbb{E}_{\nu' \sim \mathbb{Q}} \mathbb{E}_{u' \sim \nu'} \|\mathcal{G}^*(u') - \mathcal{G}(u')\|_{\mathcal{Y}}^2 \quad (3.3)$$

to be small. Other approaches to quantify OOD accuracy are possible, such as worst-case analysis.

The following corollary is useful. It is a consequence of Prop. 3.1 and the Cauchy–Schwarz inequality.

Corollary 3.2 (basic inequality). *For any $\mu \in \mathcal{P}_2(\mathcal{U})$ and maps \mathcal{G}^* and \mathcal{G} , it holds that*

$$\mathcal{E}_{\mathbb{Q}}(\mathcal{G}) \leq \mathbb{E}_{u \sim \mu} \|\mathcal{G}^*(u) - \mathcal{G}(u)\|_{\mathcal{Y}}^2 + \sqrt{\mathbb{E}_{\nu' \sim \mathbb{Q}} c^2(\mathcal{G}^*, \mathcal{G}, \mu, \nu')} \sqrt{\mathbb{E}_{\nu' \sim \mathbb{Q}} W_2^2(\mu, \nu')}. \quad (3.4)$$

The upper bound (3.4) on the average-case OOD error $\mathcal{E}_{\mathbb{Q}}$ is intuitive. We view the arbitrary probability measure μ as the training data distribution that we are free to select. The first term on the right-hand side of (3.4) then represents the in-distribution generalization error of \mathcal{G} . On the other hand, the second term can be considered a regularizer that penalizes how far μ is from \mathbb{Q} on average with respect to the W_2 metric. The factor involving the quantity c further penalizes the size of moments of μ and \mathbb{Q} as well as the size of the Lipschitz constants of \mathcal{G}^* and \mathcal{G} .

We now instantiate Cor. 3.2 in the concrete context of Gaussian mixtures.

Example 3.3 (Gaussian mixtures). Consider the *random* Gaussian measure $\nu' = \mathcal{N}(m, \mathcal{C}) \sim \mathbb{Q} \in \mathcal{P}_2(\mathcal{P}_2(\mathcal{U}))$, where $(m, \mathcal{C}) \sim \Pi$ and Π is the mixing distribution over the mean (with marginal Π_1) and covariance (with marginal Π_2). Define the Gaussian mixture $\bar{\nu} := \mathbb{E}_{(m, \mathcal{C}) \sim \Pi} \mathcal{N}(m, \mathcal{C}) \in \mathcal{P}_2(\mathcal{U})$ via duality. Let $\bar{\mu} := \mathbb{E}_{(m', \mathcal{C}') \sim \Pi'} \mathcal{N}(m', \mathcal{C}')$ be another Gaussian mixture with mixing distribution Π' (with marginals denoted by Π'_1 and Π'_2). By linearity of expectation and Fubini’s theorem, $\mathcal{E}_{\mathbb{Q}}(\mathcal{G}) = \mathcal{E}_{\bar{\nu}}(\mathcal{G})$; that is, average-case accuracy with respect to \mathbb{Q} is equivalent to accuracy with respect to the single test distribution $\bar{\nu}$. This fact and Cor. 3.2 yield $\mathcal{E}_{\mathbb{Q}}(\mathcal{G}) \leq \mathbb{E}_{u \sim \bar{\mu}} \|\mathcal{G}^*(u) - \mathcal{G}(u)\|_{\mathcal{Y}}^2 + c(\mathcal{G}^*, \mathcal{G}, \bar{\mu}, \bar{\nu})W_2(\bar{\mu}, \bar{\nu})$. The factor $c(\mathcal{G}^*, \mathcal{G}, \bar{\mu}, \bar{\nu})$ can be further simplified using the closed-form

expression for second moments of Gaussian measures. For the W_2 factor, Lem. B.1 in SM B and coupling arguments imply that

$$\mathcal{E}_{\mathbb{Q}}(\mathcal{G}) \leq \mathbb{E}_{u \sim \bar{\mu}} \|\mathcal{G}^*(u) - \mathcal{G}(u)\|_{\mathcal{Y}}^2 + c(\mathcal{G}^*, \mathcal{G}, \bar{\mu}, \bar{\nu}) \sqrt{W_2^2(\Pi_1, \Pi'_1) + W_2^2(\Pi_2, \Pi'_2)}. \quad (3.5)$$

The two W_2 distances between the marginals may be further bounded with (A.1) in SM A under additional structural assumptions on the mixing distributions; see Rmk. B.2. We often invoke this example in numerical studies with $\mathbb{Q} = \sum_{k=1}^K w_k \delta_{\nu'_k}$ (where $K \in \mathbb{N}$, i.e., a finite mixture), weights $\sum_{k=1}^K w_k = 1$, Gaussian test measures $\{\nu'_k\}$, and degenerate training mixture $\bar{\mu} := \mathcal{N}(m_0, C_0)$.

Although the preceding OOD results hold in a quite general setting, they do not distinguish between an arbitrary model and a trained model obtained by ERM (2.1). Sharpening the bounds for a trained model would require probabilistic estimates on the model’s Lipschitz constant and in-distribution error. These are challenging theoretical tasks. Instead, we turn our attention to implementable algorithms inspired by Cor. 3.2 that are designed to reduce OOD error in practice.

4 Practical algorithms for training distribution design

Let $\mathcal{G}^*: \mathcal{U} \rightarrow \mathcal{Y}$ be the target mapping and \mathbb{Q} be a probability measure over $\mathcal{P}_2(\mathcal{U})$. We assume query access to an oracle that returns the label $\mathcal{G}^*(u) \in \mathcal{Y}$ when presented with an input $u \in \mathcal{U}$. The idealized infinite data training distribution selection problem that we wish to address is

$$\inf_{\nu \in \mathcal{P}_2(\mathcal{U})} \left\{ \mathcal{E}_{\mathbb{Q}}(\widehat{\mathcal{G}}^{(\nu)}) \mid \widehat{\mathcal{G}}^{(\nu)} \in \arg \min_{\mathcal{G} \in \mathcal{H}} \mathbb{E}_{u \sim \nu} \|\mathcal{G}^*(u) - \mathcal{G}(u)\|_{\mathcal{Y}}^2 \right\}, \quad (4.1)$$

where $\mathcal{E}_{\mathbb{Q}}$ is the average-case OOD accuracy functional (3.3) and \mathcal{H} is the model hypothesis class. Eqn. (4.1) is a bilevel optimization problem. The inner minimization problem seeks the best-fit model $\widehat{\mathcal{G}}^{(\nu)}$ for a fixed training distribution ν . The outer problem minimizes $\mathcal{E}_{\mathbb{Q}}(\widehat{\mathcal{G}}^{(\nu)})$ over ν in the space of probability measures. The map $\nu \mapsto \widehat{\mathcal{G}}^{(\nu)}$ can be highly nonlinear, which poses a challenge to solve (4.1). To devise practical solution methods, this section considers the bilevel optimization problem (4.1) in Sec. 4.1 and a computationally tractable relaxation of (4.1) in Sec. 4.2.

4.1 Exact bilevel formulation

This subsection focuses on directly solving the bilevel optimization problem (4.1) to identify the optimal training distribution. Bilevel optimization has been extensively studied in the literature; see, for example, [13, 24, 53]. For the infinite-dimensional problem (4.1), our approach begins by specifying a Hilbert space \mathcal{H} . Using its linear structure, we calculate the gradient of the Lagrangian associated with (4.1) with respect to the variable ν . This gradient computation leverages the *adjoint state method* and the envelope theorem [3]. In what follows, we specialize this general framework to the case where \mathcal{H} is a reproducing kernel Hilbert space (RKHS) with scalar output space $\mathcal{Y} = \mathbb{R}$. The resulting algorithm can be efficiently implemented using representer theorems for kernel methods [38]. Additionally, other linear classes of functions can be incorporated into this framework with minimal effort. Extending the framework to nonlinear, vector-valued function spaces \mathcal{H} , such as neural network spaces, presents an exciting direction for future research.

RKHS. Let $\mathcal{H} := (\mathcal{H}_{\kappa}, \langle \cdot, \cdot \rangle_{\kappa}, \|\cdot\|_{\kappa})$ be a separable RKHS of real-valued functions on \mathcal{U} with bounded continuous reproducing kernel $\kappa: \mathcal{U} \times \mathcal{U} \rightarrow \mathbb{R}$. For fixed $\nu \in \mathcal{P}_2(\mathcal{U})$, let $\iota_{\nu}: \mathcal{H} \hookrightarrow L_{\nu}^2$ be the canonical inclusion map (which is compact under the assumptions on κ). The adjoint of the inclusion map is the kernel integral operator $\iota_{\nu}^*: L_{\nu}^2 \rightarrow \mathcal{H}$ defined by $\iota_{\nu}^* h = \int_{\mathcal{U}} \kappa(\cdot, u) h(u) \nu(du)$. We also define the self-adjoint operator $\mathcal{K}_{\nu} := \iota_{\nu}^* \iota_{\nu}: \mathcal{H} \rightarrow \mathcal{H}$, which has the same action as ι_{ν}^* .

Method of adjoints. Assume that $\mathcal{G}^* \in L_{\nu}^2 \equiv L_{\nu}^2(\mathcal{U}; \mathbb{R})$ for every $\nu \in \mathcal{P}_2(\mathcal{U})$ under consideration; this is true, for example, if \mathcal{G}^* is uniformly bounded on \mathcal{U} . Define the data misfit $\Psi: \mathcal{H} \rightarrow \mathbb{R}$ by $\Psi(\mathcal{G}) := \frac{1}{2} \|\iota_{\nu} \mathcal{G} - \mathcal{G}^*\|_{L_{\nu}^2}^2$; this is an abstract way to write the convex inner objective in (4.1) (rescaled by 1/2). By Lem. C.1, the inner solution $\widehat{\mathcal{G}}^{(\nu)}$ solves the equation $\mathcal{K}_{\nu} \widehat{\mathcal{G}}^{(\nu)} = \iota_{\nu}^* \mathcal{G}^*$ in \mathcal{H} . This fact allows us to define the Lagrangian $\mathcal{L}: \mathcal{P}_2(\mathcal{U}) \times \mathcal{H} \times \mathcal{H} \rightarrow \mathbb{R}$ for (4.1) by

$$\mathcal{L}(\nu, \mathcal{G}, \lambda) = \frac{1}{2} \mathbb{E}_{\nu' \sim \mathbb{Q}} \|\iota_{\nu'} \mathcal{G} - \mathcal{G}^*\|_{L_{\nu'}^2}^2 + \langle (\mathcal{K}_{\nu} \mathcal{G} - \iota_{\nu}^* \mathcal{G}^*), \lambda \rangle_{\kappa}. \quad (4.2)$$

Algorithm 1 Training Data Design via Gradient Descent on a Parametrized Bilevel Objective

```

1: Initialize: Parameter  $\vartheta^{(0)}$ , step sizes  $\{t_k\}$ 
2: for  $k = 0, 1, 2, \dots$  do
3:   Gradient step: With  $\nabla J$  as in (4.4), update the training distribution's parameters via
      
$$\vartheta^{(k+1)} = \vartheta^{(k)} - t_k \nabla J(\vartheta^{(k)})$$

4:   if stopping criterion is met then
5:     Return  $\vartheta^{(k+1)}$  then break
6:   end if
7: end for

```

Differentiating \mathcal{L} with respect to $\mathcal{G} \in \mathcal{H}$ leads to the adjoint equation.

Lemma 4.1 (adjoint state equation). *At a critical point of the map $\mathcal{G} \mapsto \mathcal{L}(\nu, \mathcal{G}, \lambda)$ for fixed (ν, \mathcal{G}) , the adjoint state $\lambda = \lambda^{(\nu)}(\mathcal{G}) \in \mathcal{H}$ satisfies the compact operator equation*

$$\mathcal{K}_\nu \lambda^{(\nu)}(\mathcal{G}) = \mathbb{E}_{\nu' \sim \mathbb{Q}} \mathbb{E}_{u' \sim \nu'} [\kappa(\cdot, u') (\mathcal{G}^*(u') - \mathcal{G}(u'))]. \quad (4.3)$$

The preceding results enable us to differentiate \mathcal{L} with respect to ν along the constraints of (4.1).

Proposition 4.2 (derivative: infinite-dimensional case). *Define $\mathcal{J}: \mathcal{P}_2(\mathcal{U}) \rightarrow \mathbb{R}$ by $\mathcal{J}(\nu) := \mathcal{L}(\nu, \widehat{\mathcal{G}}^{(\nu)}, \lambda^{(\nu)}(\widehat{\mathcal{G}}^{(\nu)}))$. Then, in the sense of duality, $(D\mathcal{J})(\nu) = (\widehat{\mathcal{G}}^{(\nu)} - \mathcal{G}^*) \lambda^{(\nu)}(\widehat{\mathcal{G}}^{(\nu)})$ for each ν .*

SM C.1 provides the proofs of Lem. 4.1 and Prop. 4.2.

Remark 4.3 (Wasserstein gradient flow). A nonparametric approach to solve the bilevel problem (4.1) is to derive the Wasserstein gradient flow and its Lagrangian equivalence $\dot{u} = -\nabla(D\mathcal{J})(\text{Law}(u))(u)$, where $D\mathcal{J}$ is as in Prop. 4.2. This leads to a curve of measures $t \mapsto \text{Law}(u(t))$ converging to a steady-state probability distribution. But this dynamic requires gradients of the true map \mathcal{G}^* , which may not be available or could be too expensive to compute even if available. Although beyond the scope of this paper, future work will discretize this mean-field evolution with interacting particles.

Parametrized training distributions. Although Prop. 4.2 provides the desired derivative of the bilevel problem (4.1), it does not specify how to use the derivative to compute the optimal ν . This issue is nontrivial because $\nu \in \mathcal{P}_2(\mathcal{U})$ belongs to a nonlinear metric space. One approach assumes a parametrization $\nu = \nu_\vartheta$, where $\vartheta \in \mathcal{V}$ for some separable Hilbert parameter space \mathcal{V} . Typically $\mathcal{V} \subseteq \mathbb{R}^P$ for some $P \in \mathbb{N}$. We then use the chain rule to apply Euclidean gradient-based optimization tools to solve (4.1). To this end, define $J: \mathcal{V} \rightarrow \mathbb{R}$ by $\vartheta \mapsto J(\vartheta) := \mathcal{J}(\nu_\vartheta)$, where \mathcal{J} is as in Prop. 4.2. The following theorem computes the gradient $\nabla J: \mathcal{V} \rightarrow \mathcal{V}$.

Theorem 4.4 (gradient: parametric case). *Suppose there exists a dominating measure μ_0 such that for every $\vartheta \in \mathcal{V}$, ν_ϑ has density p_ϑ with respect to μ_0 . If $(u, \vartheta) \mapsto p_\vartheta(u)$ is sufficiently regular, then*

$$\nabla J(\vartheta) = \int_{\mathcal{U}} (\widehat{\mathcal{G}}^{(\nu_\vartheta)}(u) - \mathcal{G}^*(u)) (\lambda^{(\nu_\vartheta)}(\widehat{\mathcal{G}}^{(\nu_\vartheta)}))(u) (\nabla_\vartheta \log p_\vartheta(u)) \nu_\vartheta(du). \quad (4.4)$$

In Thm. 4.4, μ_0 is typically the Lebesgue measure if $\mathcal{U} \subseteq \mathbb{R}^d$. **SM C.1** contains the proof.

Example 4.5 (Gaussian parametrization). Consider the Gaussian model $\nu_\vartheta := \mathcal{N}(m_\vartheta, \mathcal{C}_\vartheta)$ with μ_0 being the Lebesgue measure on $\mathcal{U} = \mathbb{R}^d$. Explicit calculations with Gaussian densities show that

$$\nabla_\vartheta \log p_\vartheta(u) = -\nabla_\vartheta \Phi(u, \vartheta), \quad \text{where } \Phi(u, \vartheta) := \frac{1}{2} \|\mathcal{C}_\vartheta^{-1/2}(u - m_\vartheta)\|_2^2 + \frac{1}{2} \log \det(\mathcal{C}_\vartheta). \quad (4.5)$$

The parameters ϑ of ν_ϑ can now be updated using any gradient-based optimization method. For instance, a simple Hilbert gradient flow is given by $\dot{\vartheta} = -\nabla J(\vartheta)$.

Implementation. A gradient descent scheme for the bilevel optimization problem (4.1) is summarized in Alg. 1. Alternative gradient-based optimization methods can also be explored. Discretization details for the gradient (4.4) are provided in **SM C.1**.

Algorithm 2 Training Data Design via Alternating Model Fitting and Distribution Update Steps

- 1: **Initialize:** Training data distribution $\nu^{(0)}$, estimate of the constant $R > 0$
 - 2: **for** $k = 0, 1, 2, \dots$ **do**
 - 3: **Model training:** To obtain the trained model $\widehat{\mathcal{G}}^{(k)}$, solve the optimization problem
$$\widehat{\mathcal{G}}^{(k)} \leftarrow \arg \min_{\mathcal{G} \in \mathcal{H}} \mathbb{E}_{u \sim \nu^{(k)}} \|\mathcal{G}^*(u) - \mathcal{G}(u)\|_{\mathcal{Y}}^2$$
 - 4: **Distribution update:** Update the training distribution by solving
$$\nu^{(k+1)} \leftarrow \arg \min_{\nu \in \mathcal{P}} \left\{ \mathbb{E}_{u \sim \nu} \|\mathcal{G}^*(u) - \widehat{\mathcal{G}}^{(k)}(u)\|_{\mathcal{Y}}^2 + \sqrt{\mathbb{E}_{\nu' \sim \mathbb{Q}} c_R^2(\mathcal{G}^*, \nu, \nu')} \sqrt{\mathbb{E}_{\nu' \sim \mathbb{Q}} W_2^2(\nu, \nu')} \right\}$$
 - 5: **if** stopping criterion is met **then**
 - 6: Return $(\widehat{\mathcal{G}}^{(k)}, \nu^{(k+1)})$ **then break**
 - 7: **end if**
 - 8: **end for**
-

4.2 Upper-bound minimization

Although Alg. 1 is implementable assuming query access to the ground truth map $u \mapsto \mathcal{G}^*(u)$, it is so far restricted to linear vector spaces \mathcal{H} . This subsection relaxes problem (4.1) by instead minimizing an upper bound on the objective, which is no longer a bilevel optimization problem. We then design an alternating descent algorithm that applies to any hypothesis class \mathcal{H} (e.g., neural networks and neural operators). Empirically, the alternating algorithm converges fast, often in a few iterations.

An alternating scheme. Recall the upper bound (3.4) from Cor. 3.2, which holds for any $\mu \in \mathcal{P}_2(\mathcal{U})$. The particular choice $\mu := \nu$, where ν is a candidate training data distribution, delivers a valid upper bound for the objective functional $\mathcal{E}_{\mathbb{Q}}(\widehat{\mathcal{G}}^{(\nu)})$ in (4.1). That is,

$$\mathcal{E}_{\mathbb{Q}}(\widehat{\mathcal{G}}^{(\nu)}) \leq \mathbb{E}_{u \sim \nu} \|\mathcal{G}^*(u) - \widehat{\mathcal{G}}^{(\nu)}(u)\|_{\mathcal{Y}}^2 + \sqrt{\mathbb{E}_{\nu' \sim \mathbb{Q}} c^2(\mathcal{G}^*, \widehat{\mathcal{G}}^{(\nu)}, \nu, \nu')} \sqrt{\mathbb{E}_{\nu' \sim \mathbb{Q}} W_2^2(\nu, \nu')}. \quad (4.6)$$

It is thus natural to approximate the solution to (4.1) by the minimizing distribution of the right-hand side of (4.6). The dependence of the factor c in Prop. 3.1 on the Lipschitz constant of $\widehat{\mathcal{G}}^{(\nu)}$ is hard to capture in practice. One way to circumvent this difficulty is to further assume an upper bound $\text{Lip}(\widehat{\mathcal{G}}^{(\nu)}) \leq R$ uniformly in ν for some constant $R > 0$. We define $c_R(\mathcal{G}^*, \nu, \nu')$ to be $c(\mathcal{G}^*, \widehat{\mathcal{G}}^{(\nu)}, \nu, \nu')$ with all instances of $\text{Lip}(\widehat{\mathcal{G}}^{(\nu)})$ replaced by R . The assumption of a uniform bound on the Lipschitz constant is valid for certain chosen model classes \mathcal{H} , e.g., kernels with Lipschitz feature maps or Lipschitz-constrained neural networks [25].

We denote the candidate set of training distributions by $\mathcal{P} \subseteq \mathcal{P}_2(\mathcal{U})$. Finally, the upper-bound minimization problem becomes

$$\inf_{(\nu, \mathcal{G}) \in \mathcal{P} \times \mathcal{H}} \left\{ \mathbb{E}_{u \sim \nu} \|\mathcal{G}^*(u) - \mathcal{G}(u)\|_{\mathcal{Y}}^2 + \sqrt{\mathbb{E}_{\nu' \sim \mathbb{Q}} c_R^2(\mathcal{G}^*, \nu, \nu')} \sqrt{\mathbb{E}_{\nu' \sim \mathbb{Q}} W_2^2(\nu, \nu')} \right\}. \quad (4.7)$$

Note that since only the first term of (4.7) depends on the variable \mathcal{G} , the minimizing \mathcal{G} is given by $\widehat{\mathcal{G}}^{(\nu)}$, as defined previously. This observation motivates the alternating scheme outlined in Alg. 2.

It is important to note that not all alternating algorithms have convergence guarantees, which requires a detailed understanding of the associated fixed-point operator. In contrast, the proposed Alg. 2 comes with the following convergence guarantee.

Proposition 4.6 (monotonicity). *Under Alg. 2, the objective in (4.7) is always non-increasing.*

Proof. The proof is straightforward. Line 3 ensures that the first term of the objective (4.7) does not increase, while keeping the second term constant. Next, Line 4 minimizes both terms. Iterating this argument, we deduce that the algorithm maintains a non-increasing objective value for all k . \square

Remark 4.7 (connection to Wasserstein barycenters). If the set \mathcal{P} contains distributions with uniformly bounded second moments and the first term on the right-hand side of (4.6) is uniformly bounded over

Table 1: Function approximation with bilevel Alg. 1. Reported values are mean Err for kernel regressors trained with 2^{14} labeled data samples from (i) the initial training distribution $\mathcal{N}(m_0, I_d)$ and (ii) the optimal $\mathcal{N}(m_0, \hat{\mathcal{C}})$ from Alg. 1. One standard deviation from the mean Err over 10 independent runs is also reported.

	$g_1 (d = 3)$	$g_2 (d = 2)$	$g_3 (d = 5)$	$g_3 (d = 8)$	$g_4 (d = 4)$	$g_4 (d = 5)$
$\mathcal{N}(m_0, I_d)$	0.980 ± 0.001	0.688 ± 0.009	0.754 ± 0.014	0.919 ± 0.004	0.892 ± 0.006	0.902 ± 0.004
$\mathcal{N}(m_0, \hat{\mathcal{C}})$	0.872 ± 0.006	0.016 ± 0.000	0.144 ± 0.002	0.442 ± 0.003	0.104 ± 0.009	0.320 ± 0.007

P, then the optimal value of (4.7) is bounded above by the value of another minimization problem whose solution is the 2-Wasserstein barycenter $\nu_{\mathbb{Q}} \in \mathcal{P}_2(\mathcal{U})$ of $\mathbb{Q} \in \mathcal{P}_2(\mathcal{P}_2(\mathcal{U}))$ [7, Thm 3.7, p. 444]. An analogous bound is even easier to verify for the W_1 result (3.1). Put another way, the \mathcal{G}^* -dependent solution of the proposed problem (4.7) over P (and hence also the solution of Eqn. (4.1)) is always *at least as good* as the barycenter $\nu_{\mathbb{Q}}$, which only depends on P and \mathbb{Q} .

Implementation. To implement Alg. 2, we simply replace expectations with finite averages over empirical samples. The number of samples per iteration is a hyperparameter. Line 3 in Alg. 2 is the usual model training step, i.e., Eqn. (2.1), while the distribution update step in Line 4 can be achieved in several ways. One way involves interacting particle systems derived from (Wasserstein) gradient flows over $P \subseteq \mathcal{P}_2(\mathcal{U})$. Alternatively, if the distribution is parametrized, we can optimize over the parametrization, e.g., transport maps or Gaussian means and covariances. In this case, one can apply global optimization methods or Euclidean gradient-based solvers.

To apply gradient-based optimization algorithms, we need the derivative of the objective in (4.7) with respect to ν . Up to constants, the objective takes the form $F: P \subseteq \mathcal{P}_2(\mathcal{U}) \rightarrow \mathbb{R}$, where

$$\nu \mapsto F(\nu) := \mathbb{E}_{u \sim \nu} f(u) + \sqrt{1 + m_2(\nu)} \sqrt{\mathbb{E}_{\nu' \sim \mathbb{Q}} W_2^2(\nu, \nu')} \quad (4.8)$$

and $f: \mathcal{U} \rightarrow \mathbb{R}$. The next result differentiates F ; the proof is in SM C.2.

Proposition 4.8 (derivative: infinite-dimensional case). *Let F be as in (4.8) with f and P sufficiently regular. Then for every $\nu \in P$ and $u \in \mathcal{U}$, it holds that*

$$(DF(\nu))(u) = f(u) + \frac{1}{2} \sqrt{\frac{\mathbb{E}_{\nu' \sim \mathbb{Q}} W_2^2(\nu, \nu')}{1 + m_2(\nu)}} \|u\|_{\mathcal{U}}^2 + \sqrt{\frac{1 + m_2(\nu)}{\mathbb{E}_{\nu' \sim \mathbb{Q}} W_2^2(\nu, \nu')}} \mathbb{E}_{\nu' \sim \mathbb{Q}} \phi_{\nu, \nu'}(u) \quad (4.9)$$

in the sense of duality. The potential $\phi_{\nu, \nu'}: \mathcal{U} \rightarrow \mathbb{R}$ satisfies $\phi_{\nu, \nu'} = \frac{1}{2} \|\cdot\|_{\mathcal{U}}^2 - \varphi_{\nu, \nu'}$, where $\nabla \varphi_{\nu, \nu'} = T_{\nu \rightarrow \nu'}$ and $T_{\nu \rightarrow \nu'}$ is the W_2 -optimal transport map from ν to ν' .

Taking the gradient of $u \mapsto DF(\nu)(u)$ in (4.9) yields the Wasserstein gradient, which can be utilized in Wasserstein gradient flow discretizations; see Rmk. 4.3. In the case of parametric distributions, combining Prop. 4.8 with the chain rule yields gradient descent schemes similar to those introduced in Sec. 4.1. For further details, see Lem. C.8 and its special case derived from Rmk. C.9 in SM C.2.

5 Numerical results

This section implements Alg. 1 (the bilevel gradient descent algorithm) for function approximation using kernel methods and Alg. 2 (the alternating minimization algorithm) for two operator learning tasks. Comprehensive experiment details and settings are collected in SM E.

Bilevel gradient descent algorithm. We instantiate a discretization of Alg. 1 on several function approximation benchmarks. The test functions $\mathcal{G}^* \in \{g_i\}_{i=1}^4$ each map \mathbb{R}^d to \mathbb{R} and are comprised of the Ishigami (g_1), Sobol G (g_2), and Friedmann functions (g_3, g_4). We use the kernel framework from Sec. 4.1 with \mathcal{H} the RKHS of the squared exponential kernel with a fixed scalar bandwidth hyperparameter. Also, \mathbb{Q} is an empirical measure with 10 atoms centered at fixed Gaussian measures realized by standard normally distributed means and Wishart distributed covariance matrices. A cosine annealing scheduler determines the gradient descent step sizes. The training distribution $\nu_{\vartheta} := \mathcal{N}(m_0, \mathcal{C})$ is parametrized by the covariance matrix \mathcal{C} , which we optimize using Alg. 1.

In Table 1, we report the root relative average OOD squared error $\text{Err} := (\mathcal{E}_{\mathbb{Q}}(\hat{\mathcal{G}}(\nu)) / \mathcal{E}_{\mathbb{Q}}(0))^{1/2}$ for models trained on the initial and final iterates ν_{ϑ} of Alg. 1. However, the performance gap can close

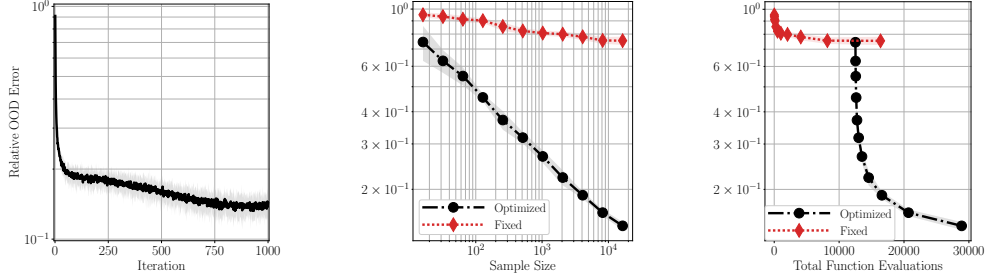


Figure 2: Alg. 1 applied to ground truth $g_3: \mathbb{R}^5 \rightarrow \mathbb{R}$. (Left) Evolution of Err over 1000 iterations of gradient descent. (Center) Err of model trained on N samples from initial ν_θ vs. optimal ν_θ . (Right) Same as center, except incorporating the additional function evaluation cost incurred from Alg. 1. Shading represents two standard deviations away from the mean over 10 independent runs.

depending on the complexity of \mathbb{Q} . Fig. 2 specializes to the g_3 case. Although fitting the model on data sampled from the optimal ν_θ seems to uniformly outperform standard normal distribution sampling, when corrected for the “offline” cost of finding the optimal ν_θ , the gains are more modest.

Alternating minimization algorithm. We apply the alternating scheme Alg. 2 to two important operator learning problems in the computational sciences. Let $\Omega \subset \mathbb{R}^2$ denote a bounded domain with boundary $\partial\Omega$. Consider the elliptic PDE $\nabla \cdot (a(x)\nabla u(x)) = 0$, where $x \in \Omega$, $a = a(x) > 0$ is the conductivity, and $u = u(x)$ is the PDE solution. Given a mean-zero Neumann boundary condition (BC) $g = a \frac{\partial u}{\partial n} |_{\partial\Omega}$, one can obtain a unique PDE solution u and the resulting Dirichlet data $f := u|_{\partial\Omega}$. For a fixed conductivity a , we define a Neumann-to-Dirichlet (NtD) map $\Lambda_a^{-1}: g \mapsto f$, which is also used in the EIT problem [18]; see also Sec. 1. On the other hand, the map $\mathcal{G}: a \mapsto u$ with a fixed Neumann or Dirichlet BC (and nonzero source) is the Darcy flow parameter-to-solution operator, which plays a crucial role in geothermal energy extraction and carbon storage applications. Learning surrogate operators for Λ_a^{-1} and \mathcal{G} can enable rapid simulations for efficient inference and control.

NtD map learning. In this example, we aim to find the optimal training distribution for learning the NtD map using the alternating minimization algorithm (AMA). The domain $\Omega = (0, 1)^2$ and the conductivity a is fixed. The meta test distribution is a mixture of K components $\mathbb{Q} = \frac{1}{K} \sum_{k=1}^K \delta_{\nu'_k}$, where each ν'_k corresponds to a distribution over g , the Neumann BC. Fig. 3 illustrates the reduction in both average relative OOD error (3.3) and relative AMA loss (4.7) over 10 iterations of Alg. 2.

Darcy flow forward map learning. We use AMA to identify the optimal training distribution for learning the Darcy flow parameter-to-solution map. Here, \mathbb{Q} is as before except now each ν'_k

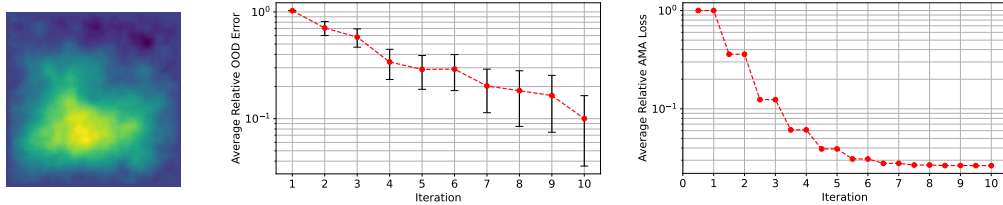


Figure 3: (Left) Conductivity for NtD learning. (Middle) After 80 independent runs, decay of the average relative OOD error of the model when trained on the optimal distribution identified at each iteration of Alg. 2; a 95% confidence interval of the true relative OOD error is provided at each iteration. (Right) Decay of average AMA loss defined in (4.7) vs. iteration relative to the same loss at initialization.

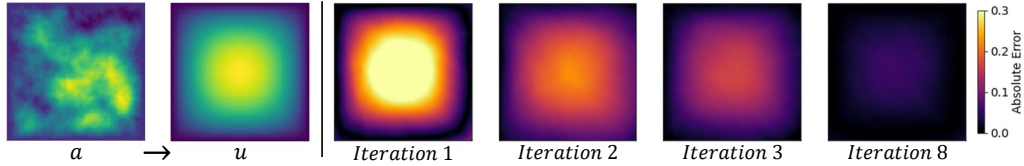


Figure 4: The first two images show the test conductivity a and true PDE solution u . The next four images show the absolute error $|u_{\text{pred}} - u|$ of the model trained on the training distribution from iterations 1, 2, 3, and 8.

represents a test distribution over the conductivity. Fig. 4 illustrates improved predictions of the neural operator trained on distributions obtained from Alg. 2 across various iterations.

6 Conclusion

This paper contributes to out-of-distribution (OOD) statistical learning analysis by introducing bilevel optimization and upper bound minimization algorithms to actively optimize training data distributions for improved OOD generalization. Rooted in the theoretical analysis, these practical methods effectively learn training distributions over target sets, as demonstrated in a proof-of-concept using simple parametric families. While the current approach shows promise, it is limited by the use of low-dimensional parametric distribution classes and the global optimization step in the alternating algorithm. Future work will address these limitations by extending the methods to higher-dimensional and nonparametric probability distribution classes, such as transport maps and empirical measures. It is also worth refining these methods using derivative-informed Wasserstein gradient flows and tackling broader challenges, including cost–accuracy trade-offs for sample allocation and iteration complexity guarantees. This work provides a solid foundation for developing robust and scalable approaches to higher-dimensional OOD generalization problems in machine learning.

Code availability

The code used to produce the numerical results and figures in this paper are available at

<https://github.com/nicolas-guerra/learning-where-to-learn>.

Acknowledgments

N.G. and Y.Y. are partially supported by the U.S. National Science Foundation (NSF) through award DMS-2409855. N.H.N. acknowledges support from NSF award DMS-2402036. The authors further acknowledge the Amazon Web Services cloud computing grant provided by Cornell University’s Center for Data Science for Enterprise and Society.

References

- [1] B. Adcock. Optimal sampling for least-squares approximation. *preprint arXiv:2409.02342*, 2024. (Cited on page 3)
- [2] B. Adcock, J. M. Cardenas, and N. Dexter. CAS4DL: Christoffel adaptive sampling for function approximation via deep learning. *Sampling Theory, Signal Processing, and Data Analysis*, 20(2):21, 2022. (Cited on page 3)
- [3] S. Afriat. Theory of maxima and the method of Lagrange. *SIAM Journal on Applied Mathematics*, 20(3):343–357, 1971. (Cited on pages 5 and 18)
- [4] P. C. Álvarez-Esteban, E. Del Barrio, J. Cuesta-Albertos, and C. Matrán. A fixed-point approach to barycenters in Wasserstein space. *Journal of Mathematical Analysis and Applications*, 441(2):744–762, 2016. (Cited on page 15)
- [5] M. Arjovsky, L. Bottou, I. Gulrajani, and D. Lopez-Paz. Invariant risk minimization. *preprint arXiv:1907.02893*, 2019. (Cited on page 2)

- [6] A. Atkinson, A. Donev, and R. Tobias. *Optimum experimental designs, with SAS*, volume 34. OUP Oxford, 2007. (Cited on page 2)
- [7] J. Backhoff-Veraguas, J. Fontbona, G. Rios, and F. Tobar. Bayesian learning with Wasserstein barycenters. *ESAIM: Probability and Statistics*, 26:436–472, 2022. (Cited on page 8)
- [8] J. A. L. Benitez, T. Furuya, F. Faucher, A. Kratsios, X. Tricoche, and M. V. de Hoop. Out-of-distributional risk bounds for neural operators with applications to the Helmholtz equation. *Journal of Computational Physics*, art. 113168, 2024. (Cited on page 15)
- [9] N. Boullé and A. Townsend. A mathematical guide to operator learning. In *Handbook of Numerical Analysis*, volume 25, pages 83–125. Elsevier, 2024. (Cited on page 3)
- [10] N. Boullé, D. Halikias, and A. Townsend. Elliptic PDE learning is provably data-efficient. *Proceedings of the National Academy of Sciences*, 120(39):e2303904120, 2023. (Cited on page 3)
- [11] S. Chewi. *Log-Concave Sampling*. Book Draft, 2024. (Cited on page 21)
- [12] J. Cockayne and A. Duncan. Probabilistic gradients for fast calibration of differential equation models. *SIAM/ASA Journal on Uncertainty Quantification*, 9(4):1643–1672, 2021. (Cited on page 17)
- [13] B. Colson, P. Marcotte, and G. Savard. An overview of bilevel optimization. *Annals of Operations Research*, 153:235–256, 2007. (Cited on page 5)
- [14] M. Dashti and A. M. Stuart. The Bayesian Approach to Inverse Problems. *Handbook of Uncertainty Quantification*, pages 311–428, 2017. (Cited on page 3)
- [15] M. V. de Hoop, N. B. Kovachki, N. H. Nelsen, and A. M. Stuart. Convergence rates for learning linear operators from noisy data. *SIAM/ASA Journal on Uncertainty Quantification*, 11(2): 480–513, 2023. (Cited on page 3)
- [16] X. Deng, W. Wang, F. Feng, H. Zhang, X. He, and Y. Liao. Counterfactual active learning for out-of-distribution generalization. In *Proceedings of the 61st Annual Meeting of the Association for Computational Linguistics (Volume 1: Long Papers)*, pages 11362–11377, 2023. (Cited on page 2)
- [17] O. R. Dunbar, N. H. Nelsen, and M. Mutic. Hyperparameter optimization for randomized algorithms: a case study on random features. *Statistics and Computing*, 35(3):1–28, 2025. (Cited on page 25)
- [18] M. M. Dunlop and A. M. Stuart. The Bayesian formulation of EIT: Analysis and algorithms. *Inverse Problems and Imaging*, 10(4):1007–1036, 2016. (Cited on page 9)
- [19] Y. Fan and L. Ying. Solving electrical impedance tomography with deep learning. *Journal of Computational Physics*, 404:109119, 2020. (Cited on page 1)
- [20] V. Fedorov. Optimal experimental design. *Wiley Interdisciplinary Reviews: Computational Statistics*, 2(5):581–589, 2010. (Cited on page 2)
- [21] A. Foster, M. Jankowiak, E. Bingham, P. Horsfall, Y. W. Teh, T. Rainforth, and N. Goodman. Variational Bayesian optimal experimental design. In *Advances in Neural Information Processing Systems*, volume 32, 2019. (Cited on page 2)
- [22] A. Garbuno-Inigo, T. Helin, F. Hoffmann, and B. Hosseini. Bayesian posterior perturbation analysis with integral probability metrics. *preprint arXiv:2303.01512*, 2023. (Cited on page 16)
- [23] M. Gelbrich. On a formula for the L^2 Wasserstein metric between measures on Euclidean and Hilbert spaces. *Mathematische Nachrichten*, 147(1):185–203, 1990. (Cited on page 14)
- [24] G. Golub and V. Pereyra. Separable nonlinear least squares: the variable projection method and its applications. *Inverse problems*, 19(2):R1, 2003. (Cited on page 5)
- [25] H. Gouk, E. Frank, B. Pfahringer, and M. J. Cree. Regularisation of neural networks by enforcing Lipschitz continuity. *Machine Learning*, 110:393–416, 2021. (Cited on page 7)
- [26] X. Huan, J. Jagalur, and Y. Marzouk. Optimal experimental design: Formulations and computations. *Acta Numerica*, 33:715–840, 2024. (Cited on page 2)
- [27] O. Kallenberg. *Random measures, theory and applications*, volume 1. Springer, 2017. (Cited on pages 3 and 14)

- [28] P. Kamath, A. Tangella, D. Sutherland, and N. Srebro. Does invariant risk minimization capture invariance? In *International Conference on Artificial Intelligence and Statistics*, pages 4069–4077. PMLR, 2021. (Cited on page 2)
- [29] N. B. Kovachki, Z. Li, B. Liu, K. Azizzadenesheli, K. Bhattacharya, A. M. Stuart, and A. Anandkumar. Neural operator: Learning maps between function spaces with applications to PDEs. *Journal of Machine Learning Research*, 24(89):1–97, 2023. (Cited on page 3)
- [30] N. B. Kovachki, S. Lanthaler, and A. M. Stuart. Operator learning: Algorithms and analysis. *Handbook of Numerical Analysis*, 25:419–467, 2024. (Cited on page 3)
- [31] S. Li, X. Yu, W. Xing, R. Kirby, A. Narayan, and S. Zhe. Multi-resolution active learning of Fourier neural operators. In *International Conference on Artificial Intelligence and Statistics*, pages 2440–2448. PMLR, 2024. (Cited on page 3)
- [32] Z. Li, N. B. Kovachki, K. Azizzadenesheli, B. Liu, K. Bhattacharya, A. M. Stuart, and A. Anandkumar. Fourier neural operator for parametric partial differential equations. In *International Conference on Learning Representations*, 2021. (Cited on pages 3 and 22)
- [33] F. Lin, X. Fang, and Z. Gao. Distributionally robust optimization: A review on theory and applications. *Numerical Algebra, Control and Optimization*, 12(1):159–212, 2022. (Cited on page 2)
- [34] Y. Lin, H. Dong, H. Wang, and T. Zhang. Bayesian invariant risk minimization. In *Proceedings of the IEEE/CVF Conference on Computer Vision and Pattern Recognition*, pages 16021–16030, 2022. (Cited on page 2)
- [35] I. Loshchilov and F. Hutter. SGDR: Stochastic Gradient Descent with Warm Restarts. In *International Conference on Learning Representations*, 2017. (Cited on page 25)
- [36] L. Lu, P. Jin, G. Pang, Z. Zhang, and G. E. Karniadakis. Learning nonlinear operators via DeepONet based on the universal approximation theorem of operators. *Nature Machine Intelligence*, 3(3):218–229, 2021. (Cited on pages 3 and 22)
- [37] N. R. Mallinar, A. Zane, S. Frei, and B. Yu. Minimum-norm interpolation under covariate shift. In *International Conference on Machine Learning*, pages 34543–34585. PMLR, 2024. (Cited on page 2)
- [38] C. A. Micchelli and M. Pontil. On learning vector-valued functions. *Neural Computation*, 17(1):177–204, 2005. (Cited on page 5)
- [39] R. Molinaro, Y. Yang, B. Engquist, and S. Mishra. Neural inverse operators for solving PDE inverse problems. In *International Conference on Machine Learning*, pages 25105–25139. PMLR, 2023. (Cited on pages 1, 2, 3, 22, and 23)
- [40] D. Musekamp, M. Kalimuthu, D. Holzmüller, M. Takamoto, and M. Niepert. Active learning for neural PDE solvers. *preprint arXiv:2408.01536*, 2024. (Cited on page 3)
- [41] N. H. Nelsen and A. M. Stuart. Operator learning using random features: A tool for scientific computing. *SIAM Review*, 66(3):535–571, 2024. (Cited on page 3)
- [42] H. Park, K. Park, S. Mo, and J. Kim. Deep neural network based electrical impedance tomographic sensing methodology for large-area robotic tactile sensing. *IEEE Transactions on Robotics*, 37(5):1570–1583, 2021. (Cited on page 1)
- [43] E. Pickering, S. Guth, G. E. Karniadakis, and T. P. Sapsis. Discovering and forecasting extreme events via active learning in neural operators. *Nature Computational Science*, 2(12):823–833, 2022. (Cited on page 3)
- [44] D. Potts and M. Schmischke. Interpretable approximation of high-dimensional data. *SIAM Journal on Mathematics of Data Science*, 3(4):1301–1323, 2021. (Cited on page 25)
- [45] H. Rahimian and S. Mehrotra. Frameworks and results in distributionally robust optimization. *Open Journal of Mathematical Optimization*, 3:1–85, 2022. (Cited on page 2)
- [46] A. Rudi, R. Camoriano, and L. Rosasco. Less is more: Nyström computational regularization. In *Advances in Neural Information Processing Systems*, volume 28, 2015. (Cited on page 17)
- [47] E. Saha, H. Schaeffer, and G. Tran. HARFE: hard-ridge random feature expansion. *Sampling Theory, Signal Processing, and Data Analysis*, 21(2):27, 2023. (Cited on page 25)
- [48] F. Santambrogio. *Optimal Transport for Applied Mathematicians: Calculus of Variations, PDEs, and Modeling*, volume 87. Birkhäuser, 2015. (Cited on pages 17, 18, and 21)

- [49] B. Settles. Active learning literature survey. Computer Sciences Technical Report 1648, University of Wisconsin–Madison, 2009. (Cited on page 2)
- [50] S. Siltanen, J. Mueller, and D. Isaacson. An implementation of the reconstruction algorithm of A. Nachman for the 2D inverse conductivity problem. *Inverse Problems*, 16(3):681, 2000. (Cited on page 22)
- [51] A. M. Stuart. Inverse problems: A Bayesian perspective. *Acta Numerica*, 19:451–559, 2010. (Cited on page 14)
- [52] U. Subedi and A. Tewari. On the benefits of active data collection in operator learning. *preprint arXiv:2410.19725*, 2024. (Cited on page 3)
- [53] T. Van Leeuwen and A. Y. Aravkin. Variable projection for nonsmooth problems. *SIAM Journal on Scientific Computing*, 43(5):S249–S268, 2021. (Cited on page 5)
- [54] C. Villani. *Topics in optimal transportation*, volume 58. American Mathematical Society, 2021. (Cited on pages 3 and 21)
- [55] Y. Yang, Y. Zhang, X. Song, and Y. Xu. Not all out-of-distribution data are harmful to open-set active learning. In *Advances in Neural Information Processing Systems*, volume 36, pages 13802–13818, 2023. (Cited on page 2)
- [56] X. Zhou, Y. Lin, W. Zhang, and T. Zhang. Sparse invariant risk minimization. In *International Conference on Machine Learning*, pages 27222–27244. PMLR, 2022. (Cited on page 2)

A Additional mathematical background

This appendix provides more mathematical background for the present work.

We begin with two comments about Gaussian distributions on Hilbert spaces. First, we remark that the 2-Wasserstein metric between Gaussian measures has a closed-form expression.

Example A.1 (2-Wasserstein metric between Gaussians). Let $\mu = \mathcal{N}(m_\mu, \mathcal{C}_\mu)$ and $\nu = \mathcal{N}(m_\nu, \mathcal{C}_\nu)$ be Gaussian measures on a real separable Hilbert space $(H, \langle \cdot, \cdot \rangle, \|\cdot\|)$. Then [23] gives

$$W_2^2(\mu, \nu) = \|m_\mu - m_\nu\|^2 + \text{tr}\left(\mathcal{C}_\mu + \mathcal{C}_\nu - 2(\mathcal{C}_\mu^{1/2}\mathcal{C}_\nu\mathcal{C}_\mu^{1/2})^{1/2}\right). \quad (\text{A.1})$$

The square root in (A.1) is the unique self-adjoint positive semidefinite (PSD) square root of a self-adjoint PSD linear operator. The trace of an operator $A: H \rightarrow H$ is given by $\text{tr}(A) = \sum_{j \in \mathbb{N}} \langle e_j, Ae_j \rangle$ for any orthonormal basis $\{e_j\}_{j \in \mathbb{N}}$ of H . If A is PSD, then we can also write $\text{tr}(A) = \|A^{1/2}\|_{\text{HS}}^2$, where $B \mapsto \|B\|_{\text{HS}}^2 := \sum_{j \in \mathbb{N}} \|Be_j\|^2$ is the squared Hilbert–Schmidt norm.

We frequently invoke (A.1) in this paper. When H is infinite-dimensional, the *Karhunen–Loève expansion* (KLE) is often useful in calculations [51, Thm. 6.19, p. 533].

Lemma A.2 (KLE of Gaussian measure). *Let $m \in (H, \langle \cdot, \cdot \rangle, \|\cdot\|)$ and $\mathcal{C}: H \rightarrow H$ be self-adjoint, PSD, and trace-class. Let $\{\lambda_j\}_{j \in \mathbb{N}} \subseteq \mathbb{R}_{\geq 0}$ be a non-increasing rearrangement of the eigenvalues of \mathcal{C} and $\{\phi_j\}_{j \in \mathbb{N}} \subseteq H$ be the corresponding orthonormal set of eigenvectors. If $\{\xi_j\}_{j \in \mathbb{N}}$ is an independent and identically distributed sequence with $\xi_1 \sim \mathcal{N}(0, 1)$, then*

$$\text{Law}\left(m + \sum_{j \in \mathbb{N}} \sqrt{\lambda_j} \xi_j \phi_j\right) = \mathcal{N}(m, \mathcal{C}). \quad (\text{A.2})$$

Generalizing Lem. A.2, there exist Karhunen–Loève expansions of non-Gaussian measures. In this case, the $\{\xi_j\}_{j \in \mathbb{N}}$ are non-Gaussian, have mean zero and variance one, and are only pairwise uncorrelated instead of independent and identically distributed (i.i.d.); still, the KLE “diagonalizes” the probability measure.

Next, we turn our attention to general probability measures on abstract spaces. This allows us to define probability measures *over* the space of probability measures.

Definition A.3 (spaces of probability measures). Let (X, \mathcal{B}) be a measurable space. The space of probability measures on X is defined by

$$\mathcal{P}(X) := \{\mu: \mathcal{B} \rightarrow [0, 1] \mid \mu \text{ is a probability measure}\}.$$

It is equipped with the σ -algebra $\mathcal{B}(\mathcal{P}(X))$ generated by the evaluation maps $e_A: \mathcal{P}(X) \rightarrow [0, 1]$ given by $e_A(\mu) := \mu(A)$ for all $A \in \mathcal{B}$. Similarly, the space of probability measures on $\mathcal{P}(X)$ is

$$\mathcal{P}(\mathcal{P}(X)) := \{\mathbb{Q}: \mathcal{B}(\mathcal{P}(X)) \rightarrow [0, 1] \mid \mathbb{Q} \text{ is a probability measure}\}.$$

Now suppose that $(\mathcal{P}(X), d)$ is a metric space. For $p \in [1, \infty)$, we say that $\mathbb{Q} \in \mathcal{P}_p(\mathcal{P}(X))$ if $\mathbb{Q} \in \mathcal{P}(\mathcal{P}(X))$ and $\mathbb{E}_{\mu \sim \mathbb{Q}}[d^p(\mu, \mu_0)] < \infty$ for some (and hence for all) $\mu_0 \in \mathcal{P}(X)$.

Def. A.3 can be related to the notion of random measure from Def. 2.2 as follows. Let $(\Omega, \mathcal{F}, \mathbb{P})$ be a probability space. Recall that a random probability measure on X is a measurable map

$$\Xi: (\Omega, \mathcal{F}) \rightarrow (\mathcal{P}(X), \mathcal{B}(\mathcal{P}(X))).$$

Then the *law* (or *distribution*) of Ξ is the pushforward measure $\text{Law}(\Xi) \in \mathcal{P}(\mathcal{P}(X))$ defined by

$$\text{Law}(\Xi)(E) := \mathbb{P}(\{\omega \in \Omega \mid \Xi(\omega) \in E\}) \quad \text{for all } E \in \mathcal{B}(\mathcal{P}(X)).$$

In this paper, we typically do not distinguish between a random measure and its law.⁴

We now provide three examples of random measures.

⁴Both concepts are closely related to *Markov kernels* [27].

Example A.4 (empirical measure). Given i.i.d. random variables X_1, \dots, X_N taking values in measurable space (M, \mathcal{B}) with $X_1 \sim \mu$, the *empirical measure* is the random probability measure $\mu^{(N)} := \frac{1}{N} \sum_{n=1}^N \delta_{X_n}$, where $\delta_x \in \mathcal{P}(M)$ is the Dirac measure at $x \in M$. For each measurable set $A \in \mathcal{B}$, the number $\mu^{(N)}(A) \in [0, 1]$ counts the fraction of samples that fall in A . The measure $\mu^{(N)}$ is random because the samples $\{X_n\}_{n=1}^N$ are random.

Example A.5 (Dirichlet process). Let α be a finite nonnegative measure on (M, \mathcal{B}) . A *Dirichlet process* $\mu \sim \text{DP}(\alpha)$ is a random probability measure such that for every k and every measurable partition $\{A_1, \dots, A_k\}$ of M , it holds that

$$(\mu(A_1), \dots, \mu(A_k)) \sim \text{Dirichlet}(\alpha(A_1), \dots, \alpha(A_k)).$$

Example A.6 (random Gaussian measures). In the infinite-dimensional state space setting, a canonical example is that of a random Gaussian measure defined through the KLE (A.2) of its mean and covariance. Let $(H, \langle \cdot, \cdot \rangle, \|\cdot\|)$ be infinite-dimensional, $\{\phi_j\}$ be an orthonormal basis of H , and $\{\lambda_j\} \subset \mathbb{R}_{\geq 0}$ and $\{\sigma_{ij}\} \subset \mathbb{R}_{\geq 0}$ be summable. Define the random measure $\mathcal{N}(m, \mathcal{C})$ by

$$m \stackrel{\text{Law}}{:=} \sum_{j \in \mathbb{N}} \sqrt{\lambda_j} \xi_j \phi_j \quad \text{and} \quad \mathcal{C} := \mathcal{R}^* \mathcal{R}, \quad \text{where} \quad \mathcal{R} \stackrel{\text{Law}}{:=} \sum_{i \in \mathbb{N}} \sum_{j \in \mathbb{N}} \sqrt{\sigma_{ij}} \zeta_{ij} \phi_i \otimes \phi_j. \quad (\text{A.3})$$

The $\{\xi_j\}$ and $\{\zeta_{ij}\}$ are zero mean, unit variance, pairwise-uncorrelated real random variables. The outer product in (A.3) is defined by $(a \otimes b)c := \langle b, c \rangle a$. Since \mathcal{R} is a KLE in the space of Hilbert-Schmidt operators on H , it follows that $\mathcal{C} = \mathcal{R}^* \mathcal{R}$ is a valid self-adjoint PSD trace-class covariance operator with probability one. Since $\{\phi_j\}$ is fixed, the degrees of freedom in $\mathbb{Q} := \text{Law}(\mathcal{N}(m, \mathcal{C}))$ are the choice of eigenvalues $\{\lambda_j\}$ and $\{\sigma_{ij}\}$ and the distribution of the coefficients $\{\xi_j\}$ and $\{\zeta_{ij}\}$. Typically the coefficients are chosen i.i.d. from some common distribution such as the standard normal distribution $\mathcal{N}(0, 1)$ or the uniform distribution on the interval $[-\sqrt{3}, \sqrt{3}]$. The preceding construction of $\mathcal{N}(m, \mathcal{C})$ immediately extends to mixtures of Gaussian measures.

To conclude **SM A**, we connect back to the barycenters described in **Rmk. 4.7**.

Definition A.7 (Wasserstein barycenter). Fix $p \in [1, \infty)$. Given a probability measure $\mathbb{Q} \in \mathcal{P}_p(\mathcal{P}_p(\mathcal{U}))$ and a set $\mathbb{P} \subseteq \mathcal{P}_p(\mathcal{U})$, a (p, \mathbb{P}) -Wasserstein barycenter of \mathbb{Q} is any solution of

$$\inf_{\mu \in \mathbb{P}} \mathbb{E}_{\nu \sim \mathbb{Q}} W_p^p(\mu, \nu). \quad (\text{A.4})$$

If $\mathbb{P} = \mathcal{P}_p(\mathcal{U})$, then we simply write p -Wasserstein barycenter for brevity.

When \mathbb{Q} is supported on Gaussian measures, the 2-Wasserstein barycenter of \mathbb{Q} can be characterized.

Example A.8 (Gaussian barycenter). Let $\mathbb{Q} := \text{Law}(\mathcal{N}(m, \mathcal{C})) \in \mathcal{P}_2(\mathcal{P}_2(\mathcal{U}))$, where $m \in \mathcal{U}$ and $\mathcal{C}: \mathcal{U} \rightarrow \mathcal{U}$ are the random mean vector and random covariance operator of a random Gaussian measure. Then the solution $\bar{\mu}$ to $\inf_{\mu \in \mathcal{P}_2(\mathcal{U})} \mathbb{E}[W_2^2(\mu, \mathcal{N}(m, \mathcal{C}))]$ is the Gaussian $\bar{\mu} = \mathcal{N}(\mathbb{E}[m], \bar{\mathcal{C}})$ [4, Thm. 2.4], where $\bar{\mathcal{C}}$ is a non-zero PSD solution to the nonlinear equation

$$\bar{\mathcal{C}} = \mathbb{E} \left[\left(\bar{\mathcal{C}}^{1/2} \mathcal{C} \bar{\mathcal{C}}^{1/2} \right)^{1/2} \right]. \quad (\text{A.5})$$

One can employ fixed-point iterations to approximately solve (A.5) for $\bar{\mathcal{C}}$.

B Details for section 3: Lipschitz theory for out-of-distribution generalization

This appendix provides the proof of **Prop. 3.1** and expands on **Ex. 3.3**. We begin with the proof.

Proof of Prop. 3.1. We begin by proving the first assertion, which is similar to the result and proof of [8, Lem. 7.2, p. 23]. Let $\phi(u) := \|\mathcal{G}_1(u) - \mathcal{G}_2(u)\|$. For any u and u' , the triangle inequality yields

$$\begin{aligned} |\phi(u) - \phi(u')| &\leq \|\mathcal{G}_1(u) - \mathcal{G}_2(u) - (\mathcal{G}_1(u') - \mathcal{G}_2(u'))\| \\ &\leq \|\mathcal{G}_2(u) - \mathcal{G}_2(u')\| + \|\mathcal{G}_1(u) - \mathcal{G}_1(u')\| \\ &\leq (\text{Lip}(\mathcal{G}_1) + \text{Lip}(\mathcal{G}_2)) \|u - u'\|. \end{aligned}$$

Thus, $\text{Lip}(\phi) \leq \text{Lip}(\mathcal{G}_1) + \text{Lip}(\mathcal{G}_2) =: C$. By Kantorovich–Rubenstein duality, $\mathbb{E}_{u' \sim \nu'} \phi(u') - \mathbb{E}_{u \sim \nu} \phi(u) \leq C W_1(\nu, \nu')$ as asserted.

For the W_2 result, note that $\|\mathcal{G}_i(u)\| \leq \text{Lip}(\mathcal{G}_i)\|u\| + \|\mathcal{G}_i(0)\|$. This and the previous estimate gives

$$\begin{aligned} \phi^2(u') - \phi^2(u) &= (\phi(u') + \phi(u))(\phi(u') - \phi(u)) \\ &\leq (\|\mathcal{G}_1(u)\| + \|\mathcal{G}_1(u')\| + \|\mathcal{G}_2(u)\| + \|\mathcal{G}_2(u')\|)C\|u - u'\| \\ &\leq (C\|u\| + C\|u'\| + 2\|\mathcal{G}_1(0)\| + 2\|\mathcal{G}_2(0)\|)C\|u - u'\|. \end{aligned}$$

Let π be the W_2 -optimal coupling of μ and μ' . By the Cauchy–Schwarz inequality, the expectation $\mathbb{E}_{u' \sim \mu'} \phi^2(u') - \mathbb{E}_{u \sim \mu} \phi^2(u) = \mathbb{E}_{(u, u') \sim \pi} [\phi^2(u') - \phi^2(u)]$ is bounded above by

$$\begin{aligned} &C \sqrt{\mathbb{E}_{(u, u') \sim \pi} (C\|u\| + C\|u'\| + 2\|\mathcal{G}_1(0)\| + 2\|\mathcal{G}_2(0)\|)^2} \sqrt{\mathbb{E}_{(u, u') \sim \pi} \|u - u'\|^2} \\ &\leq C \sqrt{4C^2(m_2(\mu) + m_2(\mu')) + 16\|\mathcal{G}_1(0)\|^2 + 16\|\mathcal{G}_2(0)\|^2} W_2(\mu, \mu'). \end{aligned}$$

The last line is due to $(a + b + c + d)^2 \leq 4(a^2 + b^2 + c^2 + d^2)$. The second assertion is proved. \square

Next, we return to Ex. 3.3 concerning Gaussian mixtures. The following lemma is used in this example; it is an independently interesting result.

Lemma B.1 (Lipschitz stability of mixtures in Wasserstein metric). *Let $p \in [1, \infty)$. If \mathbb{Q} and \mathbb{Q}' belong to $\mathcal{P}_p(\mathcal{P}_p(\mathcal{U}))$, then $W_p(\mathbb{E}_{\mu \sim \mathbb{Q}} \mu, \mathbb{E}_{\nu \sim \mathbb{Q}'} \nu) \leq W_p(\mathbb{Q}, \mathbb{Q}')$.*

Proof. Let $\Pi \in \Gamma(\mathbb{Q}, \mathbb{Q}') \subseteq \mathcal{P}(\mathcal{P}_p(\mathcal{U}) \times \mathcal{P}_p(\mathcal{U}))$ be a W_p -optimal coupling with respect to the ground space $(\mathcal{P}_p(\mathcal{U}), W_p)$. By the joint convexity of the functional W_p^p and Jensen’s inequality,

$$W_p^p(\mathbb{E}_{\mu \sim \mathbb{Q}} \mu, \mathbb{E}_{\nu \sim \mathbb{Q}'} \nu) = W_p^p(\mathbb{E}_{(\mu, \nu) \sim \Pi} \mu, \mathbb{E}_{(\mu, \nu) \sim \Pi} \nu) \leq \mathbb{E}_{(\mu, \nu) \sim \Pi} W_p^p(\mu, \nu) = W_p^p(\mathbb{Q}, \mathbb{Q}').$$

Taking p -th roots completes the proof. \square

In Lem. B.1, the Wasserstein distance $W_p(\mathbb{Q}, \mathbb{Q}')$ uses $(\mathcal{P}_p(\mathcal{U}), W_p)$ as the ground metric space in Def. 2.1. Thus, it is a Wasserstein metric over the Wasserstein space.

Last, we remark on structural assumptions that allow us to further bound (3.5) in Ex. 3.3.

Remark B.2 (KLE mixing distributions). Instate the setting and notation of Ex. 3.3. Furthermore, let $m \sim \Pi_1$ and $m' \sim \Pi'_1$ have centered (possibly non-Gaussian) KLEs

$$m \stackrel{\text{Law}}{=} \sum_{j \in \mathbb{N}} \sqrt{\lambda_j} \xi_j \phi_j \quad \text{and} \quad m' \stackrel{\text{Law}}{=} \sum_{j \in \mathbb{N}} \sqrt{\lambda'_j} \xi'_j \phi_j, \quad \text{where } \xi_j \stackrel{\text{i.i.d.}}{\sim} \eta \quad \text{and} \quad \xi'_j \stackrel{\text{i.i.d.}}{\sim} \eta'.$$

In the preceding display, we further use the notation from (A.3) in Ex. A.6; thus, $\{\xi_j\}$ and $\{\xi'_j\}$ have zero mean and unit variance, with laws in $\mathcal{P}_2(\mathbb{R})$. Let $\rho \in \Gamma(\eta, \eta')$ be the W_2 -optimal coupling. Similar to [22, Lem. 4.1, pp. 13–14], let $\pi \in \Gamma(\Pi_1, \Pi'_1)$ be a coupling with the property that $\pi = \text{Law}(h, h')$, where $h = \sum_{j \in \mathbb{N}} \sqrt{\lambda_j} z_j \phi_j$ and $h' = \sum_{j \in \mathbb{N}} \sqrt{\lambda'_j} z'_j \phi_j$ in law and $(z_j, z'_j) \stackrel{\text{i.i.d.}}{\sim} \rho$.

Then by (A.1) and the triangle inequality,

$$\begin{aligned} W_2^2(\Pi_1, \Pi'_1) &\leq \mathbb{E}_{(m, m') \sim \pi} \|m - m'\|^2 \\ &\leq 2 \mathbb{E}_\rho \sum_{j \in \mathbb{N}} \lambda_j |\xi_j - \xi'_j|^2 + 2 \mathbb{E}_{\eta'} \sum_{j \in \mathbb{N}} |\xi'_j|^2 \left| \sqrt{\lambda_j} - \sqrt{\lambda'_j} \right|^2 \\ &= 2W_2^2(\eta, \eta') \sum_{j \in \mathbb{N}} \lambda_j + 2 \sum_{j \in \mathbb{N}} \left| \sqrt{\lambda_j} - \sqrt{\lambda'_j} \right|^2. \end{aligned}$$

This estimate shows that Π_1 and Π'_1 are close in W_2 if η and η' are close in W_2 and $\{\sqrt{\lambda_j}\}$ and $\{\sqrt{\lambda'_j}\}$ are close in $\ell^2(\mathbb{N}; \mathbb{R})$. We conclude this remark by upper bounding the term $W_2^2(\Pi_1, \Pi'_1)$ appearing (3.5). Following (A.3) from Ex. A.6, suppose that $\mathcal{C} = \mathcal{R}^* \mathcal{R}$ and $\mathcal{C}' = (\mathcal{R}')^* \mathcal{R}'$, where

$$\mathcal{R} \stackrel{\text{Law}}{=} \sum_{i \in \mathbb{N}} \sum_{j \in \mathbb{N}} \sqrt{\sigma_{ij}} \zeta_{ij} \phi_i \otimes \phi_j, \quad \mathcal{R}' \stackrel{\text{Law}}{=} \sum_{i \in \mathbb{N}} \sum_{j \in \mathbb{N}} \sqrt{\sigma'_{ij}} \zeta'_{ij} \phi_i \otimes \phi_j, \quad \zeta_{ij} \stackrel{\text{i.i.d.}}{\sim} \varrho, \quad \text{and} \quad \zeta'_{ij} \stackrel{\text{i.i.d.}}{\sim} \varrho'$$

are KLE expansions in the Hilbert space $\text{HS}(\mathcal{U})$ of Hilbert–Schmidt operators from \mathcal{U} into itself. Using (A.1) and [12, Lem. SM1.2, p. SM2], it holds that

$$\begin{aligned} W_2^2(\Pi_2, \Pi'_2) &= \inf_{\gamma \in \Gamma(\Pi_2, \Pi'_2)} \mathbb{E}_{(\mathcal{C}, \mathcal{C}') \sim \gamma} W_2^2(\mathcal{N}(0, \mathcal{C}), \mathcal{N}(0, \mathcal{C}')) \\ &\leq \inf_{\gamma \in \Gamma(\Pi_2, \Pi'_2)} \mathbb{E}_\gamma \|\mathcal{R} - \mathcal{R}'\|_{\text{HS}}^2. \end{aligned}$$

Then a nearly identical coupling argument to the one used for $W_2(\Pi_1, \Pi'_1)$ delivers the bound

$$W_2^2(\Pi_2, \Pi'_2) \leq 2W_2^2(\varrho, \varrho') \sum_{i \in \mathbb{N}} \sum_{j \in \mathbb{N}} \sigma_{ij} + 2 \sum_{i \in \mathbb{N}} \sum_{j \in \mathbb{N}} \left| \sqrt{\sigma_{ij}} - \sqrt{\sigma'_{ij}} \right|^2.$$

C Details for section 4: Practical algorithms for training distribution design

This appendix expands on the content of Sec. 4 and provides the deferred proofs of the theoretical results from that section. **SM C.1** concerns the bilevel minimization algorithm from Sec. 4.1 and **SM C.2** pertains to the alternating minimization algorithm from Sec. 4.2.

C.1 Derivations for subsection 4.1: Exact bilevel formulation

Proofs. Recall the use of the adjoint method in real (i.e., $\mathcal{Y} = \mathbb{R}$) RKHS \mathcal{H} with kernel κ from Sec. 4.1. For a fixed $\nu \in \mathcal{P}_2(\mathcal{U})$, the data misfit $\Psi: \mathcal{H} \rightarrow \mathbb{R}$ for this ν is

$$\mathcal{G} \mapsto \Psi(\mathcal{G}) := \frac{1}{2} \|\iota_\nu \mathcal{G} - \mathcal{G}^*\|_{L^2_\nu(\mathcal{U})}^2 = \mathbb{E}_{u \sim \nu} |\mathcal{G}(u) - \mathcal{G}^*(u)|^2. \quad (\text{C.1})$$

This is the inner objective in (4.1). In the absence of RKHS norm penalization, typically one must assume the existence of minimizers of Ψ [46, Assump. 1, p. 3]. The next lemma characterizes them.

Lemma C.1 (inner minimization solution). *Fix a set $\mathsf{P} \subseteq \mathcal{P}_2(\mathcal{U})$ of probability measures. Suppose that for every $\nu \in \mathsf{P}$, there exists $\widehat{\mathcal{G}}^{(\nu)} \in \mathcal{H}$ such that $\Psi(\widehat{\mathcal{G}}^{(\nu)}) = \inf_{\mathcal{G} \in \mathcal{H}} \Psi(\mathcal{G})$, where Ψ is as in (C.1). Then $\widehat{\mathcal{G}}^{(\nu)}$ satisfies the compact operator equation $\mathcal{K}_\nu \widehat{\mathcal{G}}^{(\nu)} = \iota_\nu^* \mathcal{G}^*$ in \mathcal{H} .*

Proof. The result follows from convex optimization in separable Hilbert space. Since we assume minimizers of Ψ exist, they are critical points. The Frechét derivative $D\Psi: \mathcal{H} \rightarrow \mathcal{H}^*$ is

$$\mathcal{G} \mapsto D\Psi(\mathcal{G}) = \langle \iota_\nu^*(\iota_\nu \mathcal{G} - \mathcal{G}^*), \cdot \rangle_\kappa.$$

At a critical point \mathcal{G} , we have $D\Psi(\mathcal{G}) = 0$ in \mathcal{H}^* . This means

$$\langle \iota_\nu^*(\iota_\nu \mathcal{G} - \mathcal{G}^*), h \rangle_\kappa = 0 \quad \text{for all } h \in \mathcal{H}.$$

By choosing $h = \iota_\nu^*(\iota_\nu \mathcal{G} - \mathcal{G}^*)$, it follows that $\iota_\nu^* \iota_\nu \mathcal{G} = \mathcal{K}_\nu \mathcal{G} = \iota_\nu^* \mathcal{G}^*$ in \mathcal{H} as asserted. \square

Next, recall the Lagrangian \mathcal{L} from (4.2). We prove Lem. 4.1 on the adjoint state equation.

Proof of Lem. 4.1. The action of the Frechét derivative with respect to the second coordinate is

$$D_2 \mathcal{L}(\nu, \mathcal{G}, \lambda) = \mathbb{E}_{\nu' \sim \mathbb{Q}} \langle \iota_{\nu'}^*(\iota_{\nu'} \mathcal{G} - \mathcal{G}^*), \cdot \rangle_\kappa + \langle \mathcal{K}_\nu \lambda, \cdot \rangle_\kappa \in \mathcal{H}^*.$$

Setting the preceding display equal to $0 \in \mathcal{H}^*$, we deduce that

$$\mathcal{K}_\nu \lambda = \mathbb{E}_{\nu' \sim \mathbb{Q}} [\iota_{\nu'}^*(\mathcal{G}^* - \iota_{\nu'} \mathcal{G})] \quad \text{in } \mathcal{H}.$$

Simplifying the right-hand side using the definition of $\iota_{\nu'}^*$ completes the proof. \square

We are now in a position to prove Prop. 4.2, which computes the first variation of $\mathcal{J}: \nu \mapsto \mathcal{L}(\nu, \widehat{\mathcal{G}}^{(\nu)}, \lambda^{(\nu)}(\widehat{\mathcal{G}}^{(\nu)}))$ in the sense of [48, Def. 7.12, p. 262].

Proof of Prop. 4.2. The first variation [48, Def. 7.12, p. 262] of \mathcal{L} with respect to the variable ν is given by the function

$$D_1\mathcal{L}(\nu, \mathcal{G}, \lambda) = (\mathcal{G} - \mathcal{G}^*)\lambda$$

that maps from \mathcal{U} to \mathbb{R} , which is independent of ν given \mathcal{G} and λ . Now let $\widehat{\mathcal{G}}^{(\nu)}$ be as in Lem. C.1 and $\lambda^{(\nu)}$ be as in Lem. 4.1. Due to the smoothness of \mathcal{L} (4.2) with respect to both \mathcal{G} and ν —in particular, \mathcal{L} is convex in \mathcal{G} and linear in ν —the envelope theorem [3] ensures that

$$(D\mathcal{J})(\nu) = (D_1\mathcal{L})\Big|_{(\nu, \mathcal{G}, \lambda) = (\nu, \widehat{\mathcal{G}}^{(\nu)}, \lambda^{(\nu)}(\widehat{\mathcal{G}}^{(\nu)})} = (\widehat{\mathcal{G}}^{(\nu)} - \mathcal{G}^*)\lambda^{(\nu)}(\widehat{\mathcal{G}}^{(\nu)})$$

as asserted. \square

Remark C.2 (Wasserstein gradient). As discussed in Rmk. 4.3, it is clear that

$$\nabla D\mathcal{J} = (\nabla\widehat{\mathcal{G}}^{(\nu)} - \nabla\mathcal{G}^*)\lambda^{(\nu)}(\widehat{\mathcal{G}}^{(\nu)}) + (\widehat{\mathcal{G}}^{(\nu)} - \mathcal{G}^*)\nabla(\lambda^{(\nu)}(\widehat{\mathcal{G}}^{(\nu)}))$$

is the Wasserstein gradient of \mathcal{J} [48, Chp. 8.2]. Its computation requires the usual \mathcal{U} -gradient of the trained model $\widehat{\mathcal{G}}^{(\nu)}$, the true map \mathcal{G}^* , and the optimal adjoint state $\lambda^{(\nu)}(\widehat{\mathcal{G}}^{(\nu)})$.

We now turn to the parametric training distribution setting. Let $\nu = \nu_\vartheta$, where $\vartheta \in \mathcal{V}$ and $(\mathcal{V}, \langle \cdot, \cdot \rangle_{\mathcal{V}}, \|\cdot\|_{\mathcal{V}})$ is a parameter Hilbert space as introduced in Sec. 4.1. The main result of Sec. 4.1 is Thm. 4.4. Before proving that theorem, we require the following lemma.

Lemma C.3 (differentiation under the integral). *Let the density $p_\vartheta := d\nu_\vartheta/d\mu_0$ be such that $(u, \vartheta) \mapsto p_\vartheta(u)$ is sufficiently regular. Then for all bounded continuous functions $\phi \in C_b(\mathcal{U})$ and all $\vartheta \in \mathcal{V}$, it holds that*

$$\nabla_\vartheta \int_{\mathcal{U}} \phi(u) \nu_\vartheta(du) = \int_{\mathcal{U}} \phi(u) \left(\nabla_\vartheta \log p_\vartheta(u) \right) \nu_\vartheta(du). \quad (\text{C.2})$$

Proof. By the assumed smoothness and absolute continuity with respect to μ_0 ,

$$\nabla_\vartheta \int_{\mathcal{U}} \phi(u) \nu_\vartheta(du) = \int_{\mathcal{U}} \phi(u) \nabla_\vartheta p_\vartheta(u) \mu_0(du).$$

Shrinking the domain of integration to the support of ν_ϑ , multiplying and dividing the rightmost equality by $p_\vartheta(u)$, and using the logarithmic derivative formula delivers the assertion. \square

With the preceding lemma in hand, we are now able to prove Thm. 4.4.

Proof of Thm. 4.4. We use the chain rule for Fréchet derivatives to compute $DJ: \mathcal{V} \rightarrow \mathcal{V}^*$ and hence the gradient $\nabla J: \mathcal{V} \rightarrow \mathcal{V}$. Define $Z: \mathcal{V} \rightarrow \mathcal{P}_2(\mathcal{U})$ by $Z(\vartheta) = \nu_\vartheta$. Then Lem. C.3 and duality allow us to identify DZ with the (possibly signed) \mathcal{V} -valued measure

$$(DZ(\vartheta))(du) = (\nabla_\vartheta \log p_\vartheta(u)) Z(\vartheta)(du).$$

We next apply the chain rule for Fréchet derivatives to the composition $J = \mathcal{J} \circ Z$. This yields

$$DJ(\vartheta) = (D\mathcal{J})(Z(\vartheta)) \circ (DZ)(\vartheta) \in \mathcal{V}^*$$

for any $\vartheta \in \mathcal{V}$. To interpret this expression, let $\vartheta' \in \mathcal{V}$ be arbitrary. Then formally,

$$\begin{aligned} (DJ(\vartheta))(\vartheta') &= \int_{\mathcal{U}} (\widehat{\mathcal{G}}^{(Z(\vartheta))}(u) - \mathcal{G}^*(u)) (\lambda^{(Z(\vartheta))}(\widehat{\mathcal{G}}^{(Z(\vartheta))}))(u) \left\langle (DZ(\vartheta))(du), \vartheta' \right\rangle_{\mathcal{V}} \\ &= \left\langle \int_{\mathcal{U}} (\widehat{\mathcal{G}}^{(\nu_\vartheta)}(u) - \mathcal{G}^*(u)) (\lambda^{(\nu_\vartheta)}(\widehat{\mathcal{G}}^{(\nu_\vartheta)}))(u) (\nabla_\vartheta \log p_\vartheta(u)) \nu_\vartheta(du), \vartheta' \right\rangle_{\mathcal{V}}. \end{aligned}$$

The formula (4.4) for ∇J follows. \square

Discretized implementation. A practical, discretized implementation of the parametric bilevel gradient descent scheme Alg. 1 further requires regularization of compact operator equations and finite data approximations. When the inner objective of (4.1) is approximated over a finite data set, we have the following regularized solution for the model update obtained from kernel ridge regression. The lemma uses the compact vector and matrix notation $U = (u_1, \dots, u_N)^\top \in \mathcal{U}^N$, $\mathcal{G}^*(U)_n = \mathcal{G}^*(u_n)$ for every n , and $\kappa(U, U)_{ij} = \kappa(u_i, u_j)$ for every i and j .

Lemma C.4 (model update). *Fix a regularization strength $\sigma > 0$. Let $\{u_n\}_{n=1}^N \sim \nu^{\otimes N}$. Then*

$$\widehat{\mathcal{G}}_N^{(\nu, \sigma)} := \sum_{n=1}^N \kappa(\cdot, u_n) \beta_n \approx \widehat{\mathcal{G}}^{(\nu)}, \quad \text{where } \beta = (\kappa(U, U) + N\sigma^2 I_N)^{-1} \mathcal{G}^*(U) \in \mathbb{R}^N. \quad (\text{C.3})$$

Proof. To numerically update \mathcal{G} by solving $\mathcal{K}_\nu \mathcal{G} = \iota_\nu^* \mathcal{G}^*$ in \mathcal{H} for fixed ν , we first regularize the inverse with a small nugget parameter $\sigma > 0$. Then we define

$$\widehat{\mathcal{G}}^{(\nu, \sigma)} := (\mathcal{K}_\nu + \sigma^2 \text{Id}_{\mathcal{H}})^{-1} \iota_\nu^* \mathcal{G}^* = \iota_\nu^* (\iota_\nu \iota_\nu^* + \sigma^2 \text{Id}_{L^2})^{-1} \mathcal{G}^* \approx \widehat{\mathcal{G}}^{(\nu)}.$$

The second equality is due to the usual Woodbury push-through identity for compact linear operators. Let $\nu^{(N)} := \frac{1}{N} \sum_{n=1}^N \delta_{u_n}$ be the empirical measure with $u_n \stackrel{\text{i.i.d.}}{\sim} \nu$. We identify $L^2_{\nu^{(N)}}$ with \mathbb{R}^N equipped with the usual (i.e., unscaled) Euclidean norm. The action of $\mathcal{K}_{\nu^{(N)}}$ on a function $h \in \mathcal{H}$ is

$$\mathcal{K}_{\nu^{(N)}} h = \frac{1}{N} \sum_{n=1}^N \kappa(\cdot, u_n) h(u_n) =: \frac{1}{N} \kappa(\cdot, U) h(U) \quad (\text{C.4})$$

and similar for $\iota_{\nu^{(N)}}^*$ acting on \mathbb{R}^N . Define $\widehat{\mathcal{G}}_N^{(\nu, \sigma)} := \widehat{\mathcal{G}}^{(\nu^{(N)}, \sigma)}$. By the preceding displays,

$$\widehat{\mathcal{G}}_N^{(\nu, \sigma)} = \sum_{n=1}^N \kappa(\cdot, u_n) \beta_n, \quad \text{where } \beta = (\kappa(U, U) + N\sigma^2 I_N)^{-1} \mathcal{G}^*(U),$$

which recovers standard kernel ridge regression under square loss and Gaussian likelihood. This implies the asserted approximation $\widehat{\mathcal{G}}_N^{(\nu, \sigma)} \approx \widehat{\mathcal{G}}^{(\nu)}$. \square

In Lem. C.4, we expect that $\widehat{\mathcal{G}}_N^{(\nu, \sigma)} \rightarrow \widehat{\mathcal{G}}^{(\nu)}$ as $N \rightarrow \infty$ and $\sigma \rightarrow 0$. This lemma takes care of the finite data approximation of the model. Next, we tackle the adjoints.

When discretizing the integral in the gradient (4.4) with Monte Carlo sampling over the training data, we recognize that only the values of $\lambda = \lambda^{(\nu)}(\widehat{\mathcal{G}}^{(\nu)})$ at the training points are needed and not $\lambda \in \mathcal{H}$ itself. That is, we never need to query λ away from the current training data samples. The next lemma exploits this fact to numerically implement the adjoint state update.

Lemma C.5 (adjoint state update). *For $J \in \mathbb{N}$ and a sequence $\{M_j\} \subseteq \mathbb{N}$, define $\mathbb{Q}^{(J)} := \frac{1}{J} \sum_{j=1}^J \delta_{\mu_j^{(M_j)}}$, where $\mu_j^{(M_j)} := \frac{1}{M_j} \sum_{m=1}^{M_j} \delta_{v_m^j}$, $V^j := \{v_m^j\}_{m=1}^{M_j} \sim \mu_j^{\otimes M_j}$, and $\{\mu_j\}_{j=1}^J \sim \mathbb{Q}^{\otimes J}$. Then with $\widehat{\mathcal{G}}_N^{(\nu, \sigma)}$ and U as in (C.3), the adjoint values $(\lambda^{(\nu)}(\widehat{\mathcal{G}}^{(\nu)}))(U) \in \mathbb{R}^N$ are approximated by*

$$\widehat{\lambda}_{N, J}^{(\nu, \sigma)}(U) := \left(\kappa(U, U) + N\sigma^2 I_N \right)^{-1} \frac{N}{J} \sum_{j=1}^J \frac{1}{M_j} \kappa(U, V^j) \left(\mathcal{G}^*(V^j) - \widehat{\mathcal{G}}_N^{(\nu, \sigma)}(V^j) \right). \quad (\text{C.5})$$

Proof. Let $\mu \sim \mathbb{Q}$, where $\mathbb{Q} \in \mathcal{P}_2(\mathcal{P}_2(\mathcal{U}))$ is fixed. For some M , let $\mu^{(M)} = \frac{1}{M} \sum_{m=1}^M \delta_{v_m}$ be the empirical measure with $V = \{v_m\}_{m=1}^M \sim \mu^{\otimes M}$. Consider the case $J = 1$ so that $\mathbb{Q}^{(1)} = \delta_{\mu^{(M)}}$; the general case for $J > 1$ as asserted in the lemma follows by linearity. With $\nu = \nu^{(N)}$ being the empirical data measure corresponding to $U \in \mathcal{U}^N$, $\mathcal{G} = \widehat{\mathcal{G}}_N^{(\nu, \sigma)}$ being the trained model from Lem. C.4, and $\mathbb{Q}^{(1)}$ in place of \mathbb{Q} , the adjoint equation (4.3) from Lem. 4.1 is

$$\mathcal{K}_{\nu^{(N)}} \lambda = \frac{1}{M} \sum_{m=1}^M \kappa(\cdot, v_m) (\mathcal{G}^*(v_m) - \widehat{\mathcal{G}}_N^{(\nu, \sigma)}(v_m)).$$

Algorithm 3 Gradient Descent on a Parametrized Bilevel Objective: Discretized Scheme

- 1: **Initialize:** Parameter $\vartheta^{(0)}$, step sizes $\{t_k\}$, nuggets $\{\sigma_k\}$, sample sizes $\{N_k\}$, measure $\mathbb{Q}^{(J)}$
 - 2: **for** $k = 0, 1, 2, \dots$ **do**
 - 3: **Sample and label:** Construct the empirical measure $\nu_{\vartheta^{(k)}}^{(N_k)}$ and label vector $\mathcal{G}^*(U) \in \mathbb{R}^{N_k}$
 - 4: **Gradient step:** Update the training distribution's parameters via

$$\vartheta^{(k+1)} = \vartheta^{(k)} - t_k \int_{\mathcal{U}} \left(\widehat{\mathcal{G}}_{N_k}^{(\nu_{\vartheta^{(k)}}, \sigma_k)}(u) - \mathcal{G}^*(u) \right) \widehat{\lambda}_{N_k, J}^{(\nu_{\vartheta^{(k)}}, \sigma_k)}(u) (\nabla_{\vartheta} \log p_{\vartheta^{(k)}}(u)) \nu_{\vartheta^{(k)}}^{(N_k)}(du)$$
 - 5: **if** stopping criterion is met **then**
 - 6: Return $\vartheta^{(k+1)}$ **then break**
 - 7: **end if**
 - 8: **end for**
-

By evaluating the preceding display at the N data points $U = \{u_n\}_{n=1}^N$ and using (C.4), we obtain

$$\frac{1}{N} \kappa(U, U) \lambda(U) = \frac{1}{M} \kappa(U, V) (\mathcal{G}^*(V) - \widehat{\mathcal{G}}_N^{(\nu, \sigma)}(V)).$$

This is a linear equation for the unknown $\lambda(U) \in \mathbb{R}^N$. Finally, we regularize the equation by replacing $\kappa(U, U)$ with $\kappa(U, U) + \sigma^2 I_N$. We denote the solution of the resulting system by $\widehat{\lambda}_{N, 1}^{(\nu, \sigma)}(U)$, which is our desired approximation (C.5) of $(\lambda^{(\nu)}(\widehat{\mathcal{G}}^{(\nu)}))(U) \in \mathbb{R}^N$. \square

In Lem. C.5, the vector $\widehat{\lambda}_{N, J}^{(\nu, \sigma)}(U) \in \mathbb{R}^N$ depends on ν (through the empirical measure $\nu^{(N)} := \frac{1}{N} \sum_{n=1}^N \delta_{u_n}$), the regularization parameter σ , the current model $\widehat{\mathcal{G}}_N^{(\nu, \sigma)}$, and the random empirical measure $\mathbb{Q}^{(J)}$ (which itself depends on the sequence $\{M_j\}_{j=1}^J$). The formula (C.5) requires the inversion of the same regularized kernel matrix as in the model update (C.3). Thus, it is advantageous to pre-compute a factorization of this matrix so that it may be reused in the adjoint update step.

Finally, we perform the numerically implementable training data distribution update by inserting the approximations $\widehat{\mathcal{G}}_N^{(\nu, \sigma)}$ and $\widehat{\lambda}_{N, J}^{(\nu, \sigma)}(U)$ from Lems. C.4–C.5 and empirical measure $\nu_{\vartheta}^{(N)}$ into the exact gradient formula (4.4) for ∇J . This yields the approximate gradient

$$\widehat{\nabla} J(\vartheta) := \int_{\mathcal{U}} \left(\widehat{\mathcal{G}}_N^{(\nu_{\vartheta}, \sigma)}(u) - \mathcal{G}^*(u) \right) \widehat{\lambda}_{N, J}^{(\nu_{\vartheta}, \sigma)}(u) (\nabla_{\vartheta} \log p_{\vartheta}(u)) \nu_{\vartheta}^{(N)}(du), \quad (\text{C.6})$$

where $\nu_{\vartheta}^{(N)}$ is the empirical measure of the same training data points used to obtain both the trained model and adjoint state vector, and we identify the vector $\widehat{\lambda}_{N, J}^{(\nu, \sigma)}(U) \in \mathbb{R}^N$ with a function $\widehat{\lambda}_{N, J}^{(\nu, \sigma)} \in L_{\nu_{\vartheta}^{(N)}}^2$. This leads to Alg. 3. In this practical algorithm, we allow for a varying number N_k of training samples from $\nu_{\vartheta^{(k)}}$ and a varying regularization strength σ_k at each iteration k in Line 4. The integrals in (C.6) and Line 4 of Alg. 3 are with respect to the empirical measure; hence, they equal the equally-weighted average over the finite data samples that make up the empirical measure.

One limitation of the practical bilevel gradient descent scheme Alg. 3 as written is that it is negatively impacted by overfitting in the model update step, as discussed in the following remark.

Remark C.6 (overfitting and vanishing gradients). A drawback of approximating the integral in the exact gradient (4.4) with a Monte Carlo average over the i.i.d. training samples in (C.6) and Line 4 of Alg. 3 is that the resulting gradient approximation incorporates the training error residual. If the trained model overfits to the data, then this residual becomes extremely small, which slows down the convergence of gradient descent significantly. In the extreme case, the gradient vanishes if the model perfectly fits the training data. Thus, the proposed method as currently formulated would likely fail for highly overparametrized models. To address this problem, one solution is to hold out a “validation” subset of the training data pairs for the adjoint state and Monte Carlo integral calculations; the remaining data should be used to train the model. Another approach is to normalize the size of the approximate gradient by its current magnitude. This adaptive normalization aims to avoid small gradients. In the numerical experiments of Sec. 5, we use kernel ridge regression with strictly positive regularization; this prevents interpolation of the data and helps avoid the vanishing gradient issue.

C.2 Derivations for subsection 4.2: Upper-bound minimization

Recall the alternating minimization algorithm Alg. 2 from Sec. 4.2. We provide details about its numerical implementation. For gradient-based implementations, the first variation of the upper bound objective (4.8) is required. This is the content of Prop. 4.8, which we now prove.

Proof of Prop. 4.8. Since the first term $\int_{\mathcal{U}} f(u)\nu(du)$ in the objective F in (4.8) is linear in the argument ν , the first variation of that term is simply f itself [48, Def. 7.12, p. 262]. The chain rule of Euclidean calculus and a similar first variation calculation delivers the second term in the asserted derivative (4.9). The third and final term arising from the chain rule requires the first variation of $\nu \mapsto \mathbb{E}_{\nu' \sim \mathbb{Q}} W_2^2(\nu, \nu')$. By [48, Prop. 7.17, p. 264, applied with cost $c(x, y) = \|x - y\|_{\mathcal{U}}^2/2$], this first variation equals the Kantorovich potential $2\phi_{\nu, \nu'}$, where the asserted characterization of $\phi_{\nu, \nu'}$ is due to Brenier's theorem; see [11, Thm. 1.3.8, p. 27] or [54]. Finally, we exchange expectation over \mathbb{Q} and differentiation using dominated convergence due to the assumed regularity of the set \mathcal{P} . \square

The Wasserstein gradient of F is useful for interacting particle discretizations. We have the following corollary of Prop. 4.8.

Corollary C.7 (Wasserstein gradient). *Instate the hypotheses of Prop. 4.8. The Wasserstein gradient ∇DF at $\nu \in \mathcal{P} \subseteq \mathcal{P}_2(\mathcal{U})$ is given by the function mapping any $u \in \mathcal{U}$ to the vector*

$$((\nabla DF)(\nu))(u) = \nabla f(u) + \sqrt{\frac{\mathbb{E}_{\nu' \sim \mathbb{Q}} W_2^2(\nu, \nu')}{1 + m_2(\nu)}} u + \sqrt{\frac{1 + m_2(\nu)}{\mathbb{E}_{\nu' \sim \mathbb{Q}} W_2^2(\nu, \nu')}} (u - \mathbb{E}_{\nu' \sim \mathbb{Q}} T_{\nu \rightarrow \nu'}(u)).$$

Alternatively, one can derive standard gradients when working with a parametrized family $\{\nu_{\vartheta}\}_{\vartheta \in \mathcal{V}}$ of candidate training distributions. The next lemma instantiates this idea in the specific setting of a finite-dimensional Gaussian family.

Lemma C.8 (chain rule: Gaussians). *Instate the hypotheses of Prop. 4.8. Suppose that $\mathcal{U} \subseteq \mathbb{R}^d$. Let $\nu_{\vartheta} := \mathcal{N}(m_{\vartheta}, \mathcal{C}_{\vartheta})$ and $F(\vartheta) := F(\nu_{\vartheta})$, where F is given in (4.8). Write $p_{\vartheta}: \mathcal{U} \rightarrow \mathbb{R}_{\geq 0}$ for the density of ν_{ϑ} with respect to any σ -finite dominating measure. Then for any parameter $\vartheta \in \mathcal{V}$, it holds that*

$$\begin{aligned} \nabla F(\vartheta) &= \int_{\mathcal{U}} f(u) (\nabla_{\vartheta} \log p_{\vartheta}(u)) \nu_{\vartheta}(du) \\ &+ \frac{1}{2} \sqrt{\frac{\mathbb{E}_{\nu' \sim \mathbb{Q}} W_2^2(\nu_{\vartheta}, \nu')}{1 + \|m_{\vartheta}\|_{\mathcal{U}}^2 + \text{tr}(\mathcal{C}_{\vartheta})}} \int_{\mathcal{U}} \frac{\|u\|_{\mathcal{U}}^2}{2} (\nabla_{\vartheta} \log p_{\vartheta}(u)) \nu_{\vartheta}(du) \\ &+ \sqrt{\frac{1 + \|m_{\vartheta}\|_{\mathcal{U}}^2 + \text{tr}(\mathcal{C}_{\vartheta})}{\mathbb{E}_{\nu' \sim \mathbb{Q}} W_2^2(\nu_{\vartheta}, \nu')}} \int_{\mathcal{U}} \frac{1}{2} \langle u, (I_d - \mathbb{E}_{\mathbb{Q}}[A'_{\vartheta}])u \rangle_{\mathcal{U}} (\nabla_{\vartheta} \log p_{\vartheta}(u)) \nu_{\vartheta}(du) \\ &+ \sqrt{\frac{1 + \|m_{\vartheta}\|_{\mathcal{U}}^2 + \text{tr}(\mathcal{C}_{\vartheta})}{\mathbb{E}_{\nu' \sim \mathbb{Q}} W_2^2(\nu_{\vartheta}, \nu')}} \int_{\mathcal{U}} \langle u, \mathbb{E}_{\mathbb{Q}}[A'_{\vartheta}]m_{\vartheta} - \mathbb{E}_{\mathbb{Q}}[m'] \rangle_{\mathcal{U}} (\nabla_{\vartheta} \log p_{\vartheta}(u)) \nu_{\vartheta}(du), \end{aligned}$$

where $\nu' = \mathcal{N}(m', \mathcal{C}') \sim \mathbb{Q}$ is a random Gaussian and $A'_{\vartheta} := \mathcal{C}_{\vartheta}^{-1/2} (\mathcal{C}_{\vartheta}^{1/2} \mathcal{C}' \mathcal{C}_{\vartheta}^{1/2})^{1/2} \mathcal{C}_{\vartheta}^{-1/2}$.

Proof. The W_2 -optimal transport map from $\nu = \mathcal{N}(m_1, \mathcal{C}_1)$ to $\nu' = \mathcal{N}(m_2, \mathcal{C}_2)$ is

$$u \mapsto T_{\nu \rightarrow \nu'}(u) := m_2 + A(u - m_1), \quad \text{where } A := \mathcal{C}_1^{-1/2} (\mathcal{C}_1^{1/2} \mathcal{C}_2 \mathcal{C}_1^{1/2})^{1/2} \mathcal{C}_1^{-1/2}.$$

Furthermore, $\phi_{\nu, \nu'} = \|\cdot\|_{\mathcal{U}}^2/2 - \varphi_{\nu, \nu'}$, where $\nabla \varphi_{\nu, \nu'} = T_{\nu \rightarrow \nu'}$ by Brenier's theorem [11, Thm. 1.3.8, p. 27]. Upon integration, we find that

$$u \mapsto \phi_{\nu, \nu'}(u) = \frac{\|u\|_{\mathcal{U}}^2}{2} - \frac{1}{2} \langle u, Au \rangle - \langle u, m_2 - Am_1 \rangle.$$

This formula is unique up to a constant. Now let $\nu := \nu_{\vartheta} = \mathcal{N}(m_{\vartheta}, \mathcal{C}_{\vartheta})$ and $\nu' = \mathcal{N}(m', \mathcal{C}') \sim \mathbb{Q}$ be as in the hypotheses of the lemma. By the chain rule for Fréchet derivatives,

$$\nabla F(\vartheta) = \int_{\mathcal{U}} (DF(\nu_{\vartheta}))(u) (\nabla_{\vartheta} \log p_{\vartheta}(u)) \nu_{\vartheta}(du)$$

for each ϑ . Applying (4.9) from Prop. 4.8, closed-form formulas for the second moments of Gaussian distributions, and the Fubini–Tonelli theorem to exchange integrals completes the proof. \square

Lem. C.8 requires the gradient $\nabla_{\vartheta} \log p_{\vartheta}$ of the log density with respect to the parameter ϑ . In general, this gradient has no closed form and must be computed numerically, e.g., with automatic differentiation. However, when only the mean of the Gaussian family is allowed to vary, the following remark discusses an analytical expression for the gradient.

Remark C.9 (Gaussian mean parametrization). Let $\mathcal{U} \subseteq \mathbb{R}^d$. If $\vartheta = m$ so that $\nu_{\vartheta} = \nu_m = \mathcal{N}(m, \mathcal{C}_0)$ for fixed \mathcal{C}_0 , then $\nabla_m \log p_m(u) = \mathcal{C}^{-1}(u - m)$, where p_m is the Lebesgue density of ν_m .

D Operator learning architectures

In this appendix, we provide detailed descriptions of the various deep operator learning architectures used in the paper. These are the DeepONet (SM D.1), NIO (SM D.2), and the newly proposed AMINO (SM D.3).

D.1 DeepONet: Deep Operator Network

Deep operator networks (DeepONet) [36] provide a general framework for learning nonlinear operators $\mathcal{G}^* : u \mapsto \mathcal{G}^*(u)$ from data. A DeepONet \mathcal{G}_{θ} achieves this via two jointly trained subnetworks:

- **Branch network B**: takes as input the values of the input function u at a fixed set of sensor locations $\{x^{(j)}\}_{j=1}^J$ and outputs a feature vector $b \in \mathbb{R}^p$ for some fixed latent dimension p .
- **Trunk network T**: takes as input a query point z in the output domain and outputs feature vector $t(z) \in \mathbb{R}^p$.

The operator prediction at function u and query point z is then formed by the inner product of these features, yielding

$$\mathcal{G}_{\theta}(u)(z) = \langle \mathbf{B}(u(x^{(1)}), \dots, u(x^{(J)})), \mathbf{T}(z) \rangle_{\mathbb{R}^p} = \sum_{k=1}^p \mathbf{B}_k(u(x^{(1)}), \dots, u(x^{(J)})) \mathbf{T}_k(z). \quad (\text{D.1})$$

During ERM training as in (2.1), the weights θ of both neural networks B and T are optimized together to minimize the average discrepancy between $\mathcal{G}_{\theta}(u)(z)$ and ground truth values $\mathcal{G}^*(u)(z)$ over a dataset of input-output function pairs. This branch-trunk architecture enables DeepONet to approximate a broad class of operators, including the Neumann-to-Dirichlet (NtD) map in EIT and the conductivity-to-solution map in Darcy flow considered in this work; see Sec. 5 and SM E.

D.2 NIO: Neural Inverse Operator

Traditional approaches for constructing direct solvers for inverse problems, such as the D-bar method for EIT [50], have laid the foundation for direct solver approximations utilizing modern machine learning techniques. Among these, the Neural Inverse Operator (NIO) [39] framework stands out as a significant advancement. In the context of operator learning, many inverse problems can be formulated as a mapping from an operator Λ_a , dependent on a physical parameter a , to the parameter a itself, i.e., $\Lambda_a \mapsto a$. In practical scenarios, the operator Λ_a is not directly accessible; instead, we observe its action on a set of input-output function pairs $\{(f_n, g_n)\}_n$, where $g_n = \Lambda_a(f_n)$. This observation leads to a two-step problem: first, infer the operator Λ_a from the data pairs, and second, deduce the parameter a from the inferred operator. This process can be further generalized by considering the operator as a pushforward map $(\Lambda_a)_{\#}$, which transforms an input distribution μ of functions to an output distribution ν_a of functions, i.e., $(\Lambda_a)_{\#}\mu = \nu_a$; see Sec. 2 for the definition of the pushforward operation. Consequently, a measure-centric machine learning approach to solving the inverse problem can be reformulated as learning the mapping $(\mu, \nu_a) \mapsto a$.

Conditioned on a fixed input distribution μ , NIO is designed to learn mappings from output measures ν_a to functions a , i.e., $\nu_a \mapsto a$, effectively relaxing the operator-to-function problem to a distribution-to-function problem. Since direct manipulation of measures is computationally infeasible, NIO circumvents this by leveraging finite data approximations. Specifically, it utilizes a composition of DeepONets and Fourier Neural Operators (FNO) [32] to approximate the inverse mapping from an empirical measure/approximation $\hat{\nu}_a$ to the underlying parameter function a .

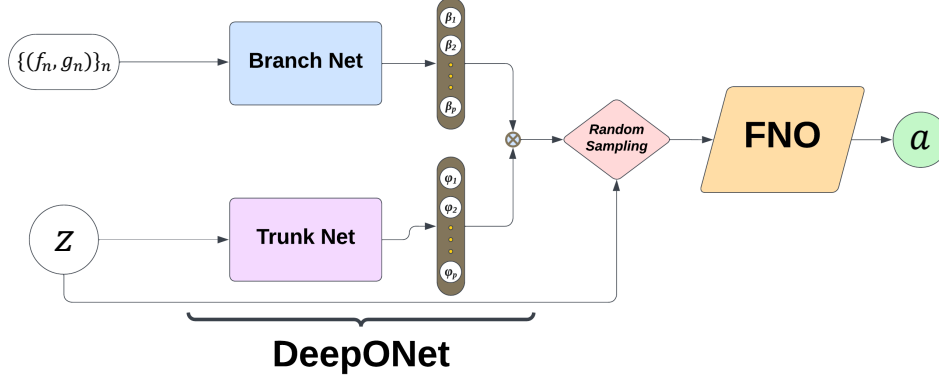


Figure 5: Schematic of the AMINO architecture, a variant of NIO, which combines a DeepONet, random sampling, and an FNO module. The model takes as input the grid point z and paired function samples $\{(f_n, g_n)\}_n$ drawn from the joint distribution $(\text{Id} \times \Lambda_a)_{\#} \mu$ and outputs the target parameter a at the point z .

D.3 AMINO: A Measure-theoretic Inverse Neural Operator

Despite the innovative architecture of NIO, it exhibits certain limitations, particularly concerning its handling of input distributions. NIO primarily focuses on the output distribution ν_a during evaluation, neglecting variability and influence of the input distribution μ . This oversight can lead to models that perform well on in-distribution (ID) data but lack robustness when faced with OOD scenarios. To address this shortcoming, we introduce *A Measure-theoretic Inverse Neural Operator* (AMINO), a framework that explicitly accounts for the input distribution in the inverse problem. By formulating the inverse task in a fully measure-theoretic setting and taking into account the input distribution, AMINO aims to improve OOD generalization. Like NIO, AMINO combines a DeepONet and an FNO. The key distinction is that AMINO incorporates both input and output functions as concatenated pairs $\{(f_n, g_n)\}_n \stackrel{\text{i.i.d.}}{\sim} (\text{Id} \times \Lambda_a)_{\#} \mu$ which are passed to the branch network, as illustrated in Fig. 5.

NIO versus AMINO. To compare the ID and OOD generalization error between NIO and AMINO, we start with the following forward problem setup taken from [39] for EIT on the domain $\Omega := (0, 1)^2 \subset \mathbb{R}^2$. The model is the two-dimensional elliptic PDE boundary value problem

$$\begin{cases} \nabla \cdot (a \nabla u) = 0 & \text{in } \Omega, \\ u = f & \text{on } \partial\Omega. \end{cases} \quad (\text{D.2})$$

For one conductivity realization a defined by

$$x \mapsto a(x) = \exp\left(\sum_{k=1}^m c_k \sin(k\pi x_1) \sin(k\pi x_2)\right), \quad (\text{D.3})$$

where $m = \lceil \bar{m} \rceil$, $\bar{m} \sim \text{Unif}([1, 5])$, and $\{c_k\} \sim \text{Unif}([-1, 1]^m)$, we take $L \in \mathbb{N}$ different Dirichlet boundary conditions $\{f_\ell\}_{\ell=1}^L$ for f in (D.2). These are given by

$$x \mapsto f_\ell(x) = \cos\left(\omega(x_1 \cos(\theta_\ell) + x_2 \sin(\theta_\ell))\right) \quad (\text{D.4})$$

with $\omega \sim \text{Unif}([\pi, 3\pi])$ and $\theta_\ell := 2\pi\ell/L$ for $\ell = 1, \dots, L$. We denote by Λ_a the DtN operator that maps the Dirichlet data of the PDE, f_ℓ , to the Neumann boundary data, $a \frac{\partial u}{\partial \mathbf{n}}|_{\partial\Omega}$, where u is the PDE solution and \mathbf{n} is the outward normal unit vector. Here, the Dirichlet boundary conditions are functions drawn from a probability distribution μ . AMINO learns the map from the joint Dirichlet–Neumann distribution $(\text{Id} \times \Lambda_a)_{\#} \mu$ to the conductivity a . In contrast, NIO only takes into account the associated Neumann data distribution $(\Lambda_a)_{\#} \mu$ as its input, with the entire neural operator conditioned on a fixed Dirichlet data distribution μ .

To compare ID generalization, both models are trained and tested on data sampled from the same Dirichlet distributions. The first two panels in Fig. 6 show that AMINO and NIO perform comparably in both training and ID settings. For OOD evaluation, the models are trained on Dirichlet data

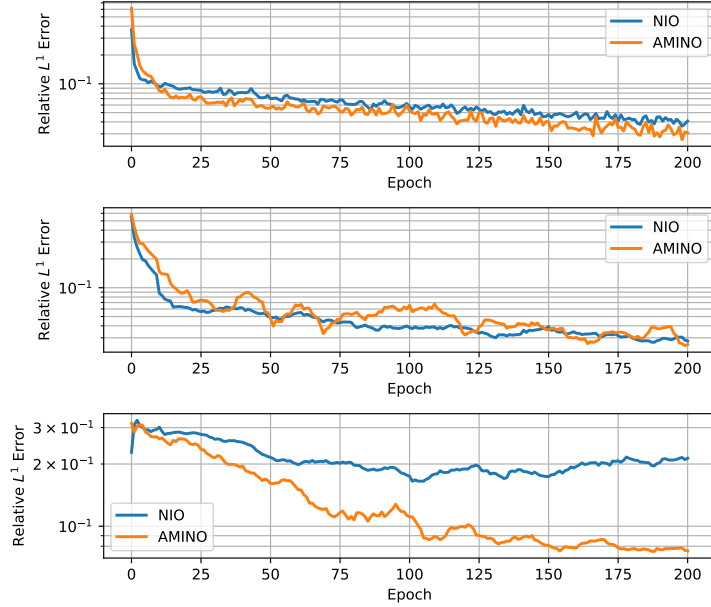


Figure 6: Training and testing performance of AMINO and NIO. (Top): Training error vs. iterations. (Middle) In-distribution testing error with $\omega \sim \text{Unif}([5\pi, \frac{11\pi}{2}])$, matching the training distribution performance. (Bottom) Out-of-distribution testing error with $\omega \sim \text{Unif}([\frac{\pi}{2}, 7\pi])$, differing from the training distribution. A rolling average with a window of 10 epochs is applied to the middle and bottom plots. AMINO demonstrates improved out-of-distribution generalization performance compared to that of the NIO framework.

with $\omega \sim \text{Unif}([5\pi, \frac{11\pi}{2}])$ and tested on data with $\omega \sim \text{Unif}([\frac{\pi}{2}, 7\pi])$. The bottom panel in Fig. 6 demonstrates that AMINO achieves significantly better OOD generalization than NIO, reducing the OOD testing error by approximately half in this example.

E Details for section 5: Numerical results

This appendix describes detailed experimental setups for all numerical tests from Sec. 1 and Sec. 5 in the main text. Regarding function approximation, SM E.1 covers the bilevel gradient descent experiments. The remaining appendices concern operator learning. SM E.2 details the AMINO experiments. SM E.3 and SM E.4 describe the results of the alternating minimization algorithm when applied to learning linear NtD maps and the nonlinear solution operator of Darcy flow, respectively.

E.1 Bilevel minimization for function approximation

We now describe the setting of the numerical results reported in Sec. 5 for Alg. 1 and its numerical version Alg. 3. Fix $m_0 \in \mathcal{U} := \mathbb{R}^d$. The goal of the experiments is to find the optimal Gaussian training distribution $\nu_\vartheta = \mathcal{N}(m_0, \mathcal{C}) \in \mathcal{P}_2(\mathbb{R}^d)$ with respect to the bilevel OOD objective (4.1), specialized to the task of function approximation. We optimize over the covariance \mathcal{C} . For all $x \in \mathbb{R}^d$, the target test functions $\mathcal{G}^* = g_i: \mathbb{R}^d \rightarrow \mathbb{R}$ for $i \in \{1, 2, 3, 4\}$ that we consider are given by

$$g_1(x) = (1 + 0.1x_3^4) \sin(x_1) + 7 \sin^2(x_2), \quad (\text{E.1})$$

$$g_2(x) = \prod_{j=1}^d \frac{|4x_j - 2| + (j - 2)/2}{1 + (j - 2)/2}, \quad (\text{E.2})$$

$$g_3(x) = 10 \sin(\pi x_1 x_2) + 20(x_3 - 1/2)^2 + 10x_4 + 5x_5, \quad \text{and} \quad (\text{E.3})$$

$$g_4(x) = \sqrt{(100x_1)^2 + \left(x_3(520\pi x_2 + 40\pi) - \frac{1}{(520\pi x_2 + 40\pi)(10x_4 + 1)} \right)^2}. \quad (\text{E.4})$$

The first two functions come from [17] and the last two from [44, 47]. They are common benchmarks in the approximation theory literature; g_1 is known as the Ishigami function, g_2 the Sobol G function, g_3 the Friedmann-1 function, and g_4 the Friedmann-2 function. Although these functions are typically defined on compact domains (e.g., $[0, 1]^d$ or $[-\pi, \pi]^d$), we instead consider approximating them on average with respect to Gaussian distributions (or mixtures thereof) on the whole of \mathbb{R}^d . We allow the dimension d to be arbitrary; in particular, the functions g_1 , g_3 , and g_4 are constant in certain directions for large enough d .

We take $m_0 = \frac{1}{2}(1, \dots, 1)^\top \in \mathbb{R}^d$ in all setups except for the one concerning test function g_2 , where we set $m_0 = 0$. Supplementary numerical results are given in Fig. 7, which reports the same information that Fig. 2 does, except now for the remaining functions $\{g_i\}$. The conclusions from these numerical results are the same. We remark that in Fig. 2, the leftmost subplot showing the training history is designed to highlight the long-time behavior (i.e., 1000 steps) of the bilevel algorithm. In practice, we only run the algorithm for $O(10)$ to $O(100)$ gradient descent iterations; this is reflected in the leftmost column of Fig. 7, where 50 steps are taken.

Model architecture and optimization algorithm. In all bilevel minimization experiments, we use the squared exponential kernel function $\kappa: \mathbb{R}^d \rightarrow \mathbb{R}_{>0}$ defined by

$$(x, x') \mapsto \kappa(x, x') := \exp\left(-\frac{\|x - x'\|_2^2}{\ell^2}\right), \quad (\text{E.5})$$

where $\ell > 0$ is a scalar lengthscale hyperparameter. While not tuned for accuracy, we do adjust ℓ on the order of $O(1)$ to $O(10)$ depending on the target function g_i to avoid blow up of the bilevel gradient descent iterations. We also experimented with the Laplace kernel $(x, x') \mapsto \exp(-\|x - x'\|_1/\ell)$; although giving similar accuracy as κ , the Laplace kernel led to slower bilevel optimization. Thus, we opted to report all results using the squared exponential kernel κ . Given a candidate set of training samples, the resulting kernel method is trained on these samples via kernel ridge regression as in Lem. C.4. We solve all linear systems with lower triangular direct solves using Cholesky factors of the regularized kernel matrices. No iterative optimization algorithms are required to train the kernel regressors. When fitting the kernel models to data outside of the bilevel gradient descent loop (see the center and right columns of Fig. 7), we set the ridge strength as $\sigma^2 = 10^{-3}/N$, where N is the current training sample size.

Training and optimization procedure. Moving on to describe the specific implementation details of Alg. 3, we initialize the covariance matrix as the identity $\vartheta^{(0)} = I_d$. We decrease the gradient descent step sizes $\{t_k\}$ in Alg. 3 according to a cosine annealing scheduler [35] with initial learning rate of 10^{-2} and final learning rate of 0. The regularization parameters $\{\sigma_k\}$ are also selected according to the cosine annealing schedule with initial value 10^{-3} and final value 10^{-7} . Although the sequence $\{N_k\}$ of training sample sizes could also be scheduled, we opt to fix $N_k = 250$ for all k in Alg. 3 for simplicity (except for when approximating g_1 , where we use $N_k = 333$). No major differences were observed when choosing $\{N_k\}$ according to cosine annealing. The identification of more principled ways to select the sequences $\{\sigma_k\}$, $\{t_k\}$, and $\{N_k\}$ to optimally balance cost and accuracy is an important direction for future work.

For the probability measure $\mathbb{Q} \in \mathcal{P}_2(\mathcal{P}_2(\mathbb{R}^d))$ over test distributions, we choose it to be the empirical measure

$$\mathbb{Q} := \frac{1}{K} \sum_{k=1}^K \delta_{\nu'_k}. \quad (\text{E.6})$$

The test measures $\nu'_k \in \mathcal{P}_2(\mathbb{R}^d)$ in (E.6) are deterministic and fixed. In applications, these could be the datasets for which we require good OOD accuracy. However, to synthetically generate the $\{\nu'_k\}$ in practice, we set

$$\nu'_k := \mathcal{N}(m'_k, C'_k), \quad \text{where } m'_k \stackrel{\text{i.i.d.}}{\sim} \mathcal{N}(0, I_d) \quad \text{and} \quad C'_k \stackrel{\text{i.i.d.}}{\sim} \text{Wishart}_d(I_d, d+1) \quad (\text{E.7})$$

for each $k = 1, \dots, K$. Once the K realizations of these distributions are generated, we view them as fixed once and for all. We assume that K and \mathbb{Q} are fixed, but we only have access to the empirical measure $\hat{\mathbb{Q}}$ defined by (E.6) but with each ν'_k replaced by the empirical measure $\frac{1}{M} \sum_{m=1}^M \delta_{\nu_m^{(k)}}$

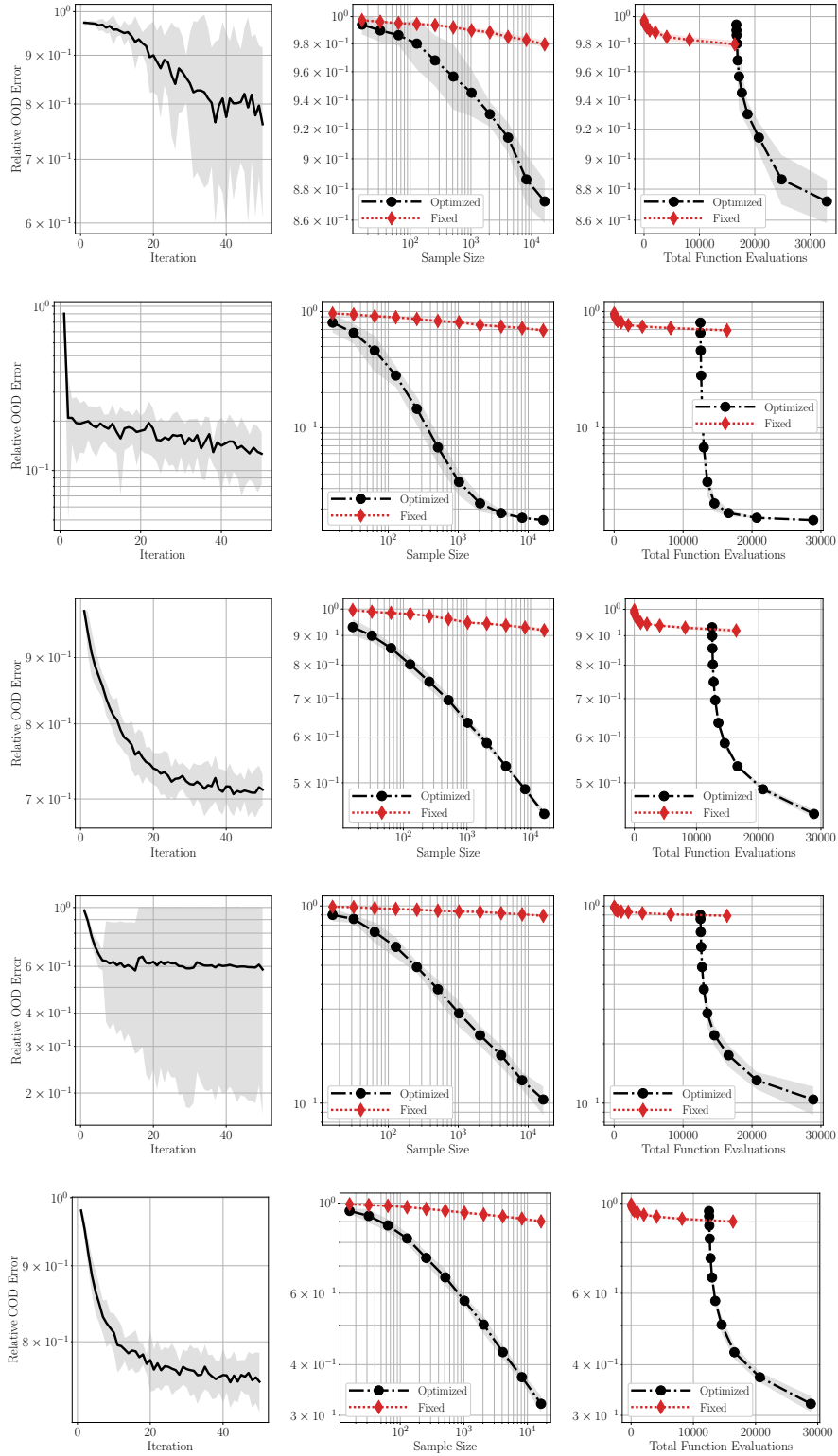


Figure 7: Bilevel Alg. 3 applied to the various ground truths $\{g_i\}$. (Left column) Evolution of Err from (E.8) over 50 gradient descent iterations. (Center column) Err of model trained on N samples from initial ν_θ vs. optimal ν_θ . (Right column) Same as center, except incorporating the additional function evaluation cost incurred from Alg. 1. From top to bottom, each row represents target functions $\{g_i\}$ corresponding to those listed in each column of Tab. 1 (from left to right, excluding g_3 in the $d = 5$ case). Shading represents two standard deviations away from the mean Err over 10 independent runs.

generated by samples $\{v_m^{(k)}\}_{m=1}^M \sim \nu_k^{\otimes M}$. In the experiments, we set $K = 10$ and $M = 5000$. To create a fair test set, we use a fixed 500 sample validation subset to update the adjoint state as in Lem. C.5 and to monitor the validation OOD accuracy during gradient descent. The remaining 4500 samples are used to evaluate the final OOD test accuracy of our trained models; see (E.8).

It remains to describe the optimization of the Gaussian family $\nu_\vartheta = \mathcal{N}(m_0, \mathcal{C})$. Practically, we actually optimize over the lower triangular Cholesky factor $\vartheta := L$ of $\mathcal{C} = LL^\top \in \mathbb{R}^{d \times d}$ instead of \mathcal{C} itself. This removes redundant parameters due to the symmetry of \mathcal{C} . We enforce strict positive definiteness of \mathcal{C} by replacing all nonpositive diagonal entries of L with a threshold value of 10^{-7} . Other than this constraint, each entry of L is optimized over the whole of \mathbb{R} . Recalling the log density formula (4.5) from Ex. 4.5, we use automatic differentiation to compute $\nabla_\vartheta \log(p_\vartheta)$; this factor appears in the definition of the approximate gradient (C.6) and in Alg. 3.

Model evaluation. We evaluate the performance of all kernel regressors $\widehat{\mathcal{G}}_N^{(\nu, \sigma)}$ regularized with strength σ^2 and trained with N i.i.d. samples from ν with respect to the root relative average OOD squared error, which is defined as

$$\text{Err} := \sqrt{\frac{\mathbb{E}_{\nu' \sim \widehat{\mathbb{Q}}} \mathbb{E}_{u' \sim \nu'} |\mathcal{G}^*(u') - \widehat{\mathcal{G}}_N^{(\nu, \sigma)}(u')|^2}{\mathbb{E}_{\nu' \sim \widehat{\mathbb{Q}}} \mathbb{E}_{u' \sim \nu'} |\mathcal{G}^*(u')|^2}} \approx \sqrt{\frac{\mathcal{E}_{\mathbb{Q}}(\widehat{\mathcal{G}}_N^{(\nu, \sigma)})}{\mathcal{E}_{\mathbb{Q}}(0)}}. \quad (\text{E.8})$$

In the preceding display, we observe that Err employs a Monte Carlo discretization of the integrals appearing in $\mathcal{E}_{\mathbb{Q}}$ by averaging over the empirical meta measure $\widehat{\mathbb{Q}}$, which is composed of $K = 10$ empirical test measures. Each individual test measure itself is an empirical measure with 4500 atoms at points that are unseen during the adjoint state calculation. See the preceding paragraph for details about our choice of \mathbb{Q} . We report values of Err in Figs. 2 and 7 and in Tab. 1.

Computational resources. All bilevel minimization experiments are performed in Python using the PyTorch framework in float32 single precision on a machine equipped with an NVIDIA GeForce RTX 4090 GPU (24 GB VRAM) running CUDA version 12.4, Intel i7-10700K CPU (8 cores/16 threads) running at 4.9 GHz, and 64 GB of DDR4-3200 CL16 RAM. The experiments required less than one total CPU and GPU hour to complete. An additional five CPU and GPU hours were expended to tune hyperparameters and set up the experiments. We ensure reproducibility of our numerical results by appropriately setting PyTorch backends to be deterministic and using fixed seeds for the relevant random number generators.

E.2 AMINO for learning electrical impedance tomography

In all machine learning tasks, the choice of training distribution plays a critical role. In practice, testing distributions can span a wide range, making training on the entire space infeasible. Instead, we must identify an optimal training distribution that enables good generalization across diverse testing scenarios.

To illustrate this, we consider the EIT problem with the AMINO solver; see SM D.3. Suppose the general distribution of interest for the Dirichlet boundary condition is generated according to the law of f_i in (D.4) with $\omega \sim \text{Unif}([\frac{\pi}{2}, 7\pi])$. A reasonable distribution to train upon is this very same distribution. However, suppose we were constrained to focus and train on distributions corresponding to $\text{Law}(\omega)$ supported only on a subset of the domain $[\frac{\pi}{2}, 7\pi]$. In that case, the choice of the distribution will greatly affect the OOD generalization error when testing with $\omega \sim \text{Unif}([\frac{\pi}{2}, 7\pi])$. To be more concrete, we will focus on four training distributions for ω , which directly determines the input Dirichlet boundary condition as in SM D.3: $\text{Unif}([\frac{\pi}{2}, \pi])$, $\text{Unif}([\frac{7\pi}{2}, 4\pi])$, $\text{Unif}([5\pi, \frac{11\pi}{2}])$, and $\text{Unif}([\frac{13\pi}{2}, 7\pi])$. After obtaining the well-trained neural operators (in the sense that the ID generalization error is small enough) corresponding to each training distribution, we study the OOD generalization error of the trained neural operators for Dirichlet data obtained by drawing $\omega \sim \text{Unif}([\frac{\pi}{2}, 7\pi])$ in (D.4).

Model architecture and optimization algorithm. We train four distinct AMINO models; see SM D.3 to recall AMINO and SM D.1 for its DeepONet component. Each model comprises three jointly trained components:

- **Branch encoder:** Eight sequential convolutional blocks with LeakyReLU activations:

- ConvBlock(1 → 64, kernel = (1, 7), stride = (1, 2), pad = (0, 3))
- ConvBlock(64 → 128, kernel = (1, 3), stride = (1, 2), pad = (0, 1))
- ConvBlock(128 → 128, kernel = (1, 3), pad = (0, 1))
- ConvBlock(128 → 256, kernel = (1, 3), stride = (1, 2), pad = (0, 1))
- ConvBlock(256 → 256, kernel = (1, 3), pad = (0, 1))
- ConvBlock(256 → 512, kernel = (1, 3), stride = (1, 2), pad = (0, 1))
- ConvBlock(512 → 512, kernel = (1, 3), pad = (0, 1))
- ConvBlock(512 → 512, kernel = (4, 5), pad = 0).

The feature map is then flattened and passed through a linear layer to produce the p -dimensional branch output.

- **Trunk network:** An 8-layer multilayer perceptron (MLP) with 512 neurons per hidden layer, LeakyReLU activations, zero dropout, and a final output dimension of $p = 100$.
- **Fourier Neural Operator (FNO):** A single spectral convolution layer with 128 channels and 32 Fourier modes.

All parameters are learned using the AdamW optimizer with a learning rate of 10^{-3} .

Training and optimization procedure. The four neural operator models “Model 1”, “Model 2”, “Model 3”, and “Model 4” are trained using four different input parameter distributions for $\text{Law}(\omega)$, respectively: $\text{Unif}([\frac{\pi}{2}, \pi])$, $\text{Unif}([\frac{7\pi}{2}, 4\pi])$, $\text{Unif}([5\pi, \frac{11\pi}{2}])$, and $\text{Unif}([\frac{13\pi}{2}, 7\pi])$; see (D.4) to recall how ω is reflected in the actual input distributions on function space. For each distribution, 4096 training samples are generated. Each sample consists of $L = 100$ Dirichlet–Neumann boundary condition pairs with the underlying conductivity discretized on a 70×70 grid for the domain $\Omega = (0, 1)^2$. After 500 training epochs, the trained models are evaluated on 1024 test samples of the distribution for the Dirichlet boundary condition (D.4) determined by $\omega \sim \text{Unif}([\frac{\pi}{2}, 7\pi])$.

Model evaluation. For both ID and OOD settings, we report the average relative L^1 error given as

$$\text{Expected Relative } L^1 \text{ Error} := \mathbb{E}_{a \sim \text{Law}(a)} \left[\frac{\|a - \mathcal{G}_\theta((\text{Id} \times \Lambda_a) \# \mu)\|_{L^1(\Omega)}}{\|a\|_{L^1(\Omega)}} \right], \quad (\text{E.9})$$

where $\text{Law}(a)$ is the distribution of a from (D.3) and \mathcal{G}_θ is the AMINO model. Using the same setup as in D.3, we approximate (E.9) with a Monte Carlo average over $N' = 1024$ test conductivity samples $a_n \stackrel{\text{i.i.d.}}{\sim} \text{Law}(a)$ and each with $L = 100$ pairs of corresponding Dirichlet and Neumann boundary data. That is, the expected relative L^1 error is approximately given by the average

$$\frac{1}{N'} \sum_{n=1}^{N'} \frac{\|a_n - \mathcal{G}_\theta\left(\frac{1}{L} \sum_{\ell=1}^L \delta_{(f_\ell^{(n)}, g_\ell^{(a_n)})}\right)\|_{L^1}}{\|a_n\|_{L^1}}, \text{ where } \{(f_\ell^{(n)}, g_\ell^{(a_n)})\}_{\ell=1}^L \sim ((\text{Id} \times \Lambda_{a_n}) \# \mu)^{\otimes L}. \quad (\text{E.10})$$

The $L^1(\Omega)$ norms in the preceding display are approximated with Riemann sum quadrature over the equally-spaced 70×70 grid.

Table 2 illustrates how OOD performance varies with the choice of training distribution. Model 1 achieves strong ID performance but performs poorly in the OOD setting. Model 2 exhibits consistent yet mediocre performance across both ID and OOD evaluations. Model 4 performs well in the ID setting but shows a noticeable drop in OOD performance. Model 3 offers the best balance, achieving low error in both ID and OOD scenarios. Notably, despite being trained on a Dirichlet data distribution with a small support regarding the parameter ω , Model 3 generalizes significantly better to the larger test domain $[\frac{\pi}{2}, 7\pi]$ for the parameter ω .

These results are further illustrated in Fig. 1, which presents two representative conductivity samples. The top row displays the predicted conductivities from each of the four models when evaluated on Dirichlet–Neumann data pairs sampled from the same distribution used during training. In this ID setting, all four models accurately recover the true conductivity. In contrast, the bottom row shows predictions when the Dirichlet data is drawn from the OOD setting, i.e., $\omega \sim \text{Unif}([\frac{\pi}{2}, 7\pi])$, and the joint Dirichlet–Neumann data distribution also changes accordingly. Under this distributional

Table 2: Average relative L^1 error of AMINO models under ID and OOD settings for the EIT inverse problem solver. Model 1 is trained on $\omega_1 \sim \text{Unif}([\frac{\pi}{2}, \pi])$, Model 2 on $\omega_2 \sim \text{Unif}([\frac{7\pi}{2}, 4\pi])$, Model 3 on $\omega_3 \sim \text{Unif}([5\pi, \frac{11\pi}{2}])$, and Model 4 on $\omega_4 \sim \text{Unif}([\frac{13\pi}{2}, 7\pi])$. In the OOD setting, all models are evaluated on Dirichlet data from $\omega \sim \text{Unif}([\frac{\pi}{2}, 7\pi])$. One standard deviation is reported. See Fig. 1 for a visual comparison on two representative samples.

	Model 1	Model 2	Model 3	Model 4
In-Distribution (ID)	0.034 ± 0.019	0.081 ± 0.028	0.021 ± 0.010	0.017 ± 0.009
Out-of-Distribution (OOD)	0.796 ± 0.251	0.078 ± 0.047	0.066 ± 0.038	0.132 ± 0.047

shift, Models 1, 2, and 4 exhibit noticeable degradation in performance, while Model 3 maintains a reasonable level of accuracy. We use this test to demonstrate the importance of carefully selecting the training data distribution to achieve robust OOD generalization.

Computational resources. The AMINO experiment was conducted on a machine equipped with an AMD Ryzen 9 5950X CPU (16 cores / 32 threads), 128 GB of RAM, and an NVIDIA RTX 3080Ti GPU (10 GB VRAM) running with CUDA version 12.1. Twelve CPU and GPU hours total were needed for the training and testing of all four models.

E.3 NtD linear operator learning

In this example from Sec. 5, we begin by defining a conductivity field $a: \Omega \subset \mathbb{R}^2 \rightarrow \mathbb{R}$ given by

$$x \mapsto a(x) = \exp\left(\sum_{j=1}^{M+1} \sum_{k=1}^{M+1} \frac{2\sigma}{((j\pi)^2 + (k\pi)^2 + \tau^2)^{\alpha/2}} z_{jk} \sin(j\pi x_1) \sin(k\pi x_2)\right) \quad (\text{E.11})$$

with fixed parameters $\alpha = 2$, $\tau = 3$, $\sigma = 3$ and random coefficients $z_{jk} \stackrel{\text{i.i.d.}}{\sim} \mathcal{N}(0, 1)$. Once these random coefficients are drawn, they are fixed throughout the example. Thus, in this experiment, our realization of the conductivity a remains fixed; see the left panel of Fig. 3 for a visualization of this a . Our goal is to develop neural operator approximations of the NtD linear operator $\mathcal{G}^* := \Lambda_a^{-1}$ that maps the Neumann boundary condition to the Dirichlet boundary condition according to the PDE (D.2) (with Neumann data g given instead of Dirichlet data f). Using the alternating minimization algorithm (AMA, Alg. 2) from Sec. 4.2, we want to optimize the training distribution over the Neumann boundary conditions to achieve small OOD generalization error (3.3).

To evaluate the OOD generalization error, we need to assign a random measure \mathbb{Q} . Let $\mathbb{Q} = \frac{1}{K} \sum_{k=1}^K \delta_{\nu'_k}$, where $\{\nu'_k\}_{k=1}^K$ are distributions over functions. For a fixed k , the function $g \sim \nu'_k$ is a Neumann boundary condition. It takes the form $g: \partial\Omega \rightarrow \mathbb{R}$, where

$$t \mapsto g(r(t)) = 10 \sin(\omega_k(t - \frac{1}{2})) + \sum_{j=1}^{N_{\text{basis}}} \frac{\sigma_k}{((j\pi)^2 + \tau_k^2)^{\alpha_k/2}} z_j \sqrt{2} \sin(j\pi t). \quad (\text{E.12})$$

We view $r: [0, 1] \rightarrow \partial\Omega$ as a 1D parametrization of the boundary $\partial\Omega \subset \mathbb{R}^2$ for the domain $\Omega := (0, 1)^2$. The entire domain is discretized on an $M \times M$ grid, where M is as in (E.11). Here $z_j \stackrel{\text{i.i.d.}}{\sim} \mathcal{N}(0, 1)$, $\alpha_k = 1.5$ for all k , and $N_{\text{basis}} = 4M - 4$. We set the grid parameter to be $M = 128$ and sample $K = 64$ test distributions in this example. The parameters $\omega_k \stackrel{\text{i.i.d.}}{\sim} \rho([-2\pi, 2\pi])$ and $\tau_k \stackrel{\text{i.i.d.}}{\sim} \rho([0, 50])$ are sampled from a custom distribution $\rho = \rho([x_{\min}, x_{\max}])$ and held fixed throughout the algorithm. The custom distribution ρ has the probability density function

$$p(x) = C \sin(x - \frac{\pi}{2}) + 1 \quad (\text{E.13})$$

for $x \in [x_{\min}, x_{\max}] \subset \mathbb{R}$, where C is a normalizing constant ensuring that p integrates to 1 over the domain $[x_{\min}, x_{\max}]$. Samples are generated by using inverse transform sampling. Any time a Neumann boundary condition g is sampled according to (E.12) and (E.13), we subtract the spatial mean of g from itself to ensure that the resulting function integrates to zero. This is necessary to make the Neumann PDE problem—as well as the NtD operator itself—well-posed.

The training distribution ν is assumed to generate functions of the form

$$t \mapsto \tilde{g}(t) = 10 \sin(\omega(t - \frac{1}{2})) + \sum_{j=1}^{N_{\text{basis}}} \frac{\sigma}{((j\pi)^2 + \tau^2)^{\alpha/2}} \tilde{z}_j \sqrt{2} \sin(j\pi t), \quad (\text{E.14})$$

where $\tilde{z}_j \stackrel{\text{i.i.d.}}{\sim} \mathcal{N}(0, 1)$, $\alpha = 2$, $\tau = 3$, and $\sigma = \tau^{3/2}$. That is, $\nu = \text{Law}(\tilde{g})$ with \tilde{g} as in (E.14). The frequency parameter ω appearing in the mean term of (E.14) is optimized using Alg. 2 to identify a training distribution that minimizes average OOD generalization error with respect to \mathbb{Q} .

Note that g and \tilde{g} are finite-term truncations of the KLE of Gaussian measures with Matérn-like covariance operators; recall Lem. A.2. In particular, for \tilde{g} , and similarly for g , the covariance operator of the Gaussian measure has eigenpairs

$$\lambda_j = \frac{\sigma^2}{((j\pi)^2 + \tau^2)^\alpha} \quad \text{and} \quad t \mapsto \phi_j(t) = \sqrt{2} \sin(j\pi t) \quad \text{for} \quad j = 1, 2, \dots, N_{\text{basis}}. \quad (\text{E.15})$$

Using (E.15) and (A.1), the squared 2-Wasserstein distance in Prop. 3.1 reduces to

$$W_2^2(\nu, \nu'_k) = \int_0^1 \left(10 \sin(\omega(t - \frac{1}{2})) - 10 \sin(\omega_k(t - \frac{1}{2})) \right)^2 dt + \sum_{j=1}^{N_{\text{basis}}} \left(\sqrt{\lambda_j} - \sqrt{\lambda_{j,k}} \right)^2, \quad (\text{E.16})$$

where $\lambda_{j,k} = \sigma_k^2 / ((j\pi)^2 + \tau_k^2)^{\alpha_k}$. We approximate the integral with standard quadrature rules. Moreover, the second moment of ν , and similarly for ν'_k , is

$$m_2(\nu) = \int_0^1 \left(10 \sin(\omega(t - \frac{1}{2})) \right)^2 dt + \sum_{j=1}^{N_{\text{basis}}} \lambda_j. \quad (\text{E.17})$$

These closed-form reductions follow directly from the finite-dimensional KLE and Ex. A.1.

Furthermore, we estimate the Lipschitz constants of both the true NtD operator \mathcal{G}^* and the learned model \mathcal{G}_θ —which appear in the multiplicative factor c from Prop. 3.1—by sampling 250 realizations of Neumann input function pairs (g_1, g_2) from 11 candidate distributions ν . We denote the finite set of these pairs of realizations by S . We then use the quantity

$$\max_{(g_1, g_2) \in S} \frac{\|\mathcal{G}(g_1) - \mathcal{G}(g_2)\|_{L^2(\partial\Omega)}}{\|g_1 - g_2\|_{L^2(\partial\Omega)}} \quad (\text{E.18})$$

to estimate the Lipschitz constant of $\text{map } \mathcal{G} \in \{\mathcal{G}^*, \mathcal{G}_\theta\}$. These Lipschitz constants are then fixed throughout the algorithm.

Model architecture and optimization algorithm. The model architecture is a DeepONet comprising a branch network with five fully connected layers of sizes $4M - 4$, 512, 512, 512, and 200, and a trunk network with five fully connected layers of sizes 2, 128, 128, 128, and 200, respectively; see SM D.1 for details. All layers use ReLU activation functions. Weights are initialized using the Glorot normal initializer. The model is trained with the Adam optimizer with a learning rate of 10^{-3} . After the model-training half step in the alternating minimization scheme Alg. 2, the parameter ω in (E.14) is optimized using SciPy’s default implementation of differential evolution with a tolerance of 10^{-7} . Due to the presence of many local minima in the optimization landscape, this global optimization algorithm is necessary.

Training and optimization procedure. The initial value for ω is set to 8π . For every model-training step, 500 pairs of Neumann and Dirichlet data are generated using the current value of ω . For practical reasons, the model is initially trained for 2000 iterations of Adam. If the AMA loss has not improved relative to the previous iteration, training continues for an additional 2000 iterations. This process is repeated up to 10 times, after which the algorithm proceeds to the parameter optimization step for the training distribution ν . During distribution parameter optimization, the AMA loss is evaluated using 500 newly generated data pairs, used specifically to compute the first term of the objective (4.7). To ensure deterministic behavior, the 500 sets of random coefficients $\{z_j\}_{j=1}^{N_{\text{basis}}}$ are fixed separately for training and optimization. This results in 1000 total sets of coefficients fixed for the entire algorithm. This process is repeated across 80 independent runs using the same conductivity but different realizations of the random coefficients $\{z_j\}$. The relative AMA loss and relative OOD error is computed for each run; see (E.19).

Model evaluation. The relative AMA loss is defined as the algorithm’s objective value (4.7) normalized by its initial value. The middle panel of Fig. 3 illustrates the rapid decay of this normalized loss over subsequent iterations. The relative OOD loss is defined as

$$\text{Relative OOD Error} := \frac{\mathbb{E}_{\nu' \sim \mathbb{Q}} \mathbb{E}_{g \sim \nu'} \|\mathcal{G}^* g - \mathcal{G}_\theta(g)\|_{L^2(\partial\Omega)}^2}{\mathbb{E}_{\nu' \sim \mathbb{Q}} \mathbb{E}_{g \sim \nu'} \|\mathcal{G}^* g\|_{L^2(\partial\Omega)}^2}, \quad (\text{E.19})$$

which measures the squared prediction error of the model \mathcal{G}_θ relative to the ground truth NtD operator \mathcal{G}^* on average with respect to the given random measure \mathbb{Q} .

The relative OOD error is estimated using Monte Carlo sampling with $K = 64$ and $N' = 500$ as

$$\text{Relative OOD Error} \approx \frac{\frac{1}{K} \sum_{k=1}^K \frac{1}{N'} \sum_{n=1}^{N'} \|\mathcal{G}^* g_{k,n} - \mathcal{G}_\theta(g_{k,n})\|_{L^2(\partial\Omega)}^2}{\frac{1}{K} \sum_{k=1}^K \frac{1}{N'} \sum_{n=1}^{N'} \|\mathcal{G}^* g_{k,n}\|_{L^2(\partial\Omega)}^2}, \quad (\text{E.20})$$

where $g_{k,n}$ is the n^{th} i.i.d. sample from ν'_k . Further numerical quadrature is used to discretize the $L^2(\partial\Omega)$ norms in the preceding display.

After 80 independent runs of Alg. 2, a 95% confidence interval for the true relative OOD error was computed using a Student’s t -distribution as seen in the middle panel of Fig. 3.

Computational resources. The computational resources here are the same as those reported in SM E.2, except three total CPU and GPU hours were needed for all independent runs.

E.4 Darcy flow forward operator learning

In this final example from Sec. 5, we are interested in learning another operator that is relevant and related to the EIT problem. In contrast with the previous example in SM E.3 where we fix the conductivity, the Darcy flow forward operator that we consider is nonlinear and maps the conductivity function a to the PDE solution u of

$$\begin{cases} -\nabla \cdot (a \nabla u) = 1 & \text{in } \Omega, \\ u = 0 & \text{on } \partial\Omega. \end{cases} \quad (\text{E.21})$$

That is, $\mathcal{G}^* : a \mapsto u$. Here, $\Omega := (0, 1)^2$.

Again, we first assign a random measure \mathbb{Q} to evaluate the OOD performance. We take $\mathbb{Q} = \frac{1}{K} \sum_{k=1}^K \delta_{\nu'_k}$, where each test distribution ν'_k is defined by parameters sampled i.i.d. from custom distributions (E.13): $m_k \sim \rho([0, 1])$, $\alpha_k \sim \rho([2, 3])$, and $\tau_k \sim \rho([1, 4])$. The scaling parameter is set as $\sigma_k = \tau_k^{\alpha_k - 1}$. We set $K = 20$ and the grid parameter $M = 64$. Given these parameters, each random conductivity function a' from test distribution ν'_k has the form

$$x \mapsto a'(x) = \exp\left(m_k + \sum_{i=1}^{M+1} \sum_{j=1}^{M+1} \frac{2\sigma_k}{((i\pi)^2 + (j\pi)^2 + \tau_k^2)^{\alpha_k/2}} z'_{ij} \sin(i\pi x_1) \sin(j\pi x_2)\right), \quad (\text{E.22})$$

where $z'_{ij} \sim \mathcal{N}(0, 1)$ independently. Sample conductivities a from training distribution ν are assumed to follow the same form

$$x \mapsto a(x) = \exp\left(m + \sum_{i=1}^{M+1} \sum_{j=1}^{M+1} \frac{2\sigma}{((i\pi)^2 + (j\pi)^2 + \tau^2)^{\alpha/2}} z_{ij} \sin(i\pi x_1) \sin(j\pi x_2)\right) \quad (\text{E.23})$$

with fixed parameters $\alpha = 2$, $\tau = 3$, and $\sigma = 3$ and $z_{ij} \stackrel{\text{i.i.d.}}{\sim} \mathcal{N}(0, 1)$. Alg. 2 is used to optimize the mean shift parameter $m \in \mathbb{R}$ in order to reduce the OOD generalization error. As in SM E.3, $\log(a)$ is modeled via a finite KLE of a Gaussian measure with Matérn-like covariance operator. Thus, by working with $\log(a)$ directly, we can exploit (A.1) to write the squared 2-Wasserstein distance factor in objective (4.7) in closed-form.

Model architecture and optimization algorithm. The same DeepONet architecture and training setup from SM E.3 are used here, except the branch network has layer sizes $M^2, 256, 256, 128$, and 200. After the model-training half step in Alg. 2, the scalar parameter m is optimized using PyTorch’s Adam optimizer with a learning rate of 10^{-3} .

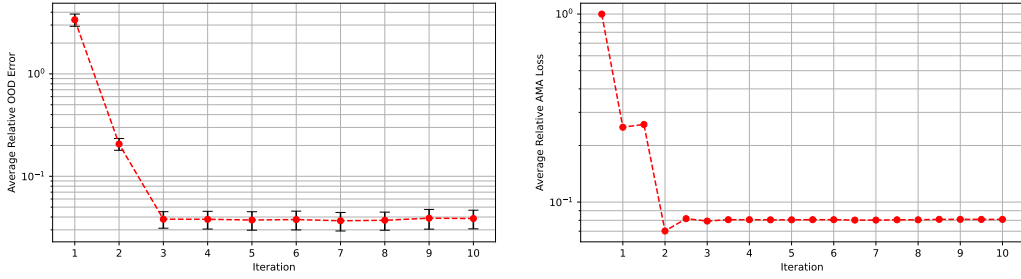


Figure 8: Average relative OOD error and average relative loss of Alg. 2 on the Darcy flow forward problem. (Left) After 13 independent runs, decay of the average relative OOD error of the model when trained on the optimal distribution identified at each iteration; a 95% confidence interval of the true relative OOD error is provided at each iteration. (Right) Decay of average AMA loss defined in (4.7) vs. iteration relative to the same loss at initialization.

Training and optimization procedure. The initial value of m is set to zero. The training and optimization procedure follows the same structure as in SM E.3, but with the following differences: 200 conductivity–solution pairs are generated for training using the current value of m . The model is initially trained for 5000 iterations. If the AMA loss has not improved relative to the previous iteration, training continues for an additional 5000 iterations. This process is repeated up to three times, after which the algorithm proceeds to the distribution parameter optimization step. During distribution parameter optimization, 500 steps are taken. Then the AMA loss is evaluated using three newly generated data pairs. If the AMA loss has not improved relative to the previous iteration, another 500 steps are taken, up to 1500 total steps. After this, the procedure returns to model training again. To ensure deterministic behavior, 203 sets of random coefficients $\{z_{ij}\}$ are fixed across training and optimization. The preceding process is repeated across 13 independent runs, each using different realizations of the coefficients. The average relative OOD error and average relative AMA loss are computed for each run.

Model evaluation. After 13 independent runs, the average relative OOD error and relative AMA loss are computed and are shown in Fig. 8. In Fig. 4, we visualize the pointwise absolute error for iterations 1, 2, 3, and 8. At these iterations, the DeepONet model is trained using the optimal training distribution produced by AMA. The model is then evaluated on the same fixed test conductivity. The progressive reduction in the spatial error across these panels of Fig. 4 corroborates the quantitative decrease in the relative OOD error, which converges to approximately 4% in our final model.

Computational resources. The computational resources here are the same as those reported in SM E.3, except three total CPU and GPU hours were needed for all independent runs.